Contrasting styles of seafloor spreading in the Woodlark Basin: Indications of rift-induced secondary mantle convection*

Fernando Martinez[1], Brian Taylor[2], and Andrew Goodliffe[2]
School of Ocean and Earth Science and Technology, University of Hawaii, Honolulu, Hawaii

Abstract. The Woodlark Basin in the southwest Pacific is a young ocean basin formed since ~6 Ma by westward stepping seafloor spreading following the rifting of continental and arc lithosphere. The N-S striking Moresby Transform divides the oceanic basin into eastern and western parts which have contrasting characteristics. Seafloor spreading west of Moresby Transform began after ~2 Ma and although spreading rates decrease to the west, the western basin has faster-spreading characteristics than the eastern basin. These include: (a) ~500 m shallower seafloor; (b) Bouguer gravity anomalies that are > 30 mGals lower; (c) magnetic anomaly and modeled seafloor magnetization amplitudes that are higher; (d) a spreading center with an axial high in contrast to the axial valleys of the eastern basin; (e) smoother seafloor fabric; and (f) exclusively non-transform spreading center offsets in contrast to the eastern basin which has transform faults and fracture zones that extend across most of the basin. Overall depth contrasts and Bouguer anomalies can be matched by end member models of thicker crust (~2 km) or thinner lithospheric (<~1/3) in the western basin. Correlated with these contrasts, the surrounding rifted margins abruptly thicken westward of the longitude of Moresby Transform. We examine alternative explanations for these contrasts and propose that rift-induced secondary mantle convection driven by thicker western margin lithosphere is most consistent with the observations. Although rift-induced convection has been cited as a cause for the voluminous excess magmatism at some rifted margins, the observations in the Woodlark Basin suggest that this mechanism may significantly affect the morphology, structure and geophysical characteristics of young ocean basins in alternate ways which resemble increased spreading rate.

1. Introduction

Observations at passive margins show widely varying conditions in the early development of ocean basins. At one extreme some "non-volcanic" margins exhibit predominantly tectonic extension with little magmatically accreted oceanic crust developed at continental breakup, leading to mantle and serpentinized ultramafic rocks exposed at the seafloor [*Leg 173 Shipboard Scientific Party*, 1998]. In these cases, numerical modeling studies [*Alvarez et al.*, 1984; *Pedersen and Ro*, 1992] suggest that slow opening rates enhance horizontal conductive cooling and may suppress or prevent melt production. At the other extreme "volcanic" margins are characterized by large volumes of intruded or subareally erupted magmas [*Mutter et al.*, 1982] where initial oceanic crustal thicknesses can exceed 25 km [*Holbrook and Kelemen*, 1993]. In both cases production of more typical thickness of oceanic crust follows this early phase after a few Ma. Although thermal anomalies in the mantle such as hot spots may explain some of the volcanic margins several examples (such as along the U.S. East Coast and in the north Atlantic) are either far from hotspot sources or geochemical and seismic studies indicate insufficient excess temperature to explain the volumes of melt produced [*Holbrook and Kelemen*, 1993; *Holbrook et al.*, 1992; *Kelemen and Holbrook*, 1995; *Zehnder et al.*, 1990]. In some cases transitions from volcanic to non-volcanic breakup occur along single margins and the character of the early ocean basin appears to be correlated with margin structure [*Mutter et al.*, 1988; *Hopper et al.*, 1992; *Keen and Potter*, 1995]. A model of rift-induced convection has been proposed [*Buck*, 1986; *Keen*, 1985] in which the geometry of the thermal boundary layer between rifting continental lithosphere and upwelling asthenosphere controls the development and intensity of secondary convection. This

*In press, 1999.
[1]Hawaii Institute of Geophysics and Planetology
[2]Department of Geology and Geophysics

component of mantle flux augments that required by passive plate separation and can bring in additional heat and increase the volume of melt produced relative to passive advection.

Although the dynamics of induced convection are poorly understood, its effects have been proposed to influence both the continental rift stage [*Buck*, 1986; *Moretti and Chénet*, 1987; *Steckler*, 1985; *Steckler et al.*, 1998] and early seafloor spreading stage [*Holbrook and Kelemen*, 1993; *Keen and Potter*, 1995; *Mutter et al.*, 1988; *Zehnder et al.*, 1990] of ocean basin development. The seismic velocity structure of several of these volcanic margins is consistent with oceanic crust [*Mutter et al.*, 1988]. The thick magmatic layers believed to be caused by induced convection are, in places, associated with the East Cost Magnetic Anomaly (ECMA) [*Holbrook and Kelemen*, 1993; *Keen and Potter*, 1995; *Kelemen and Holbrook*, 1995] and elsewhere with seafloor spreading lineations [*Hopper et al.*, 1992; *Mutter et al.*, 1988; *Mutter et al.*, 1982]. These observations indicate that the anomalous magmatism spans the rift to spreading transition and persists for an estimated 3 to 8 m.y. after breakup [*Hopper et al.*, 1992; *Kelemen and Holbrook*, 1995] within the seafloor spreading stage before typical oceanic crustal thicknesses develop. Rift-induced convection has also been proposed in environments that are completely intra-oceanic where a ridge jump into old oceanic lithosphere can produce the horizontal temperature gradients needed to initiate convection and generate excess magmatism [*Mutter et al.*, 1988].

A difficulty in studying early ocean basin development is that there are few active examples and most studies therefore focus on ancient passive margins. Although these margins have experienced the entire process of rifting, breakup, and initiation of spreading, the record of these events is not always decipherable with possibly important dynamic effects long ceased and thermal equilibration having largely occurred. In many cases these ancient margins are also buried beneath thick sediments masking or obscuring important basement characteristics, in particular the morphology and structure of the earliest formed oceanic crust. In the Woodlark Basin, a progressive and young continental breakup and currently active rift-to-spreading transition allows an examination of early ocean basin development and possible transient effects that are not evident in ancient margins. Extensive swath bathymetric and geophysical coverage and generally thin sediments allow details of the early ocean basin development to be observed. In addition, differences in the pre-rift tectonic history of the margins created a significant along-strike change in their thickness and width allowing an examination of the effects of margin geometry on the subsequent development of the oceanic basin. Although all the bordering rifted margins of the Woodlark basin can be classified as "non-volcanic" the intervening oceanic basins exhibit large contrasts in morphology and geophysical characteristics which correlate with changes in margin structure.

In this paper we use bathymetry, gravity, and magnetics data to document differences between the basins and to estimate crustal thickness variations in the surrounding rifted margins. We assess the differences between the oceanic parts of the basin in terms of crustal thickness and lithospheric thermal structure and discuss alternative possible causes for these differences. We propose that the model of rift-induced convection is the most consistent with the observations, and that it constitutes a significant control on crustal accretion at the rift to spreading transition and in early seafloor spreading development even within "non-volcanic" margins.

2. Geologic background

The Woodlark Basin (Figure 1) is a small ocean basin located between the easternmost Papuan Peninsula and the Solomon Islands in the southwest Pacific. It is bordered to the north and south by rifted margins forming the Woodlark and Pocklington Rises respectively, which were once continuous paleo-extensions of the Papuan Peninsula. The pre-rift evolution of the margins involved subduction and arc construction followed by collision and suturing of continental and arc terrains. The Trobriand Trough, bounding the western Woodlark Rise to the north and west of ~153.3°E, is a Neogene southward directed subduction zone slowly consuming the Solomon seafloor [*Davies et al.*, 1984]. To the east of Woodlark Island, the boundary between the Woodlark Rise and the Solomon Sea is a transform fault accommodating differential subduction between the Solomon Sea and Woodlark Basin at the New Britain trench [*Taylor and Exon*, 1987; *Weissel et al.*, 1982]. To the south, a Paleogene convergent boundary which accommodated northward subduction bordered what is now the Pocklington Rise and Papuan Peninsula. During the opening of the Coral Sea basin (~62-56 Ma), marginal continental plateaus rifted from Australia were transported northward on the subducting

oceanic plate, collided with, and partially underthrust the Paleogene arc along this boundary [*Weissel and Watts*, 1979]. However, an important tectonic contrast in this margin occurs near the longitude of what is now Moresby Transform (154.2°E). Underthrust continental crust extends from the Papuan Peninsula eastward to Rossel Island [*Rogerson et al.*, 1987] near 154.2°E. The emplacement of continental fragments has eliminated the trench and its free-air gravity expression within this area (see Figures 2 and 3). Farther to the east, however, the Louisiade Plateau failed to reach and therefore did not underthrust the eastern proto-Woodlark/Pocklington Rise before subduction ended [*Weissel and Watts*, 1979]. A now extinct rifted arc and trench make up the Pocklington Rise and Trough in this area [*Karig*, 1972] and the former subduction zone is still marked by a bathymetric trough and free air gravity low (Figures 2 and 3). Thus, the pre-rift tectonic setting of the eastern and western margins differed significantly with both margins originating as a volcanic arc due to northward Coral Sea subduction but the western margin additionally experienced collision and underthrusting by continental plateaus.

The current extensional phase split the rheologically weak continental/arc massif of the proto-Woodlark/Pocklington Rises that lay between stronger surrounding oceanic lithosphere of the Coral and Solomon Seas [*Benes et al.*, 1994; *Taylor et al.*, 1995, 1999]. The westward pointing wedge-shaped geometry of the basin, the westward narrowing of oceanic crust, and the overall pole of opening of the basin calculated at 9.3°S, 147°E prior to 0.52 Ma [*Taylor et al.*, 1999] indicate rifting and spreading rates have always been slower to the west. The easternmost and earliest formed oceanic part of the Woodlark Basin has being subducted beneath the Solomon arc at the New Britain and San Cristobal trenches. Existing magnetics data have been compiled and isochron identifications made from a seafloor magnetization inversion presented in *Taylor et al*. [1999] which forms the basis for the summary presented here. The oldest magnetic anomalies (An. 3A.1) in the extreme southeast of the oceanic basin indicate that seafloor spreading began by 6 Ma [*Taylor et al.*, 1999]. Spreading has subsequently transgressed westward, stepping across Simbo Transform (156.5°E) about 4 Ma and Moresby Transform (154.2°E) about 1.9 Ma to reach its current tip at 151.7°E [*Taylor et al.*, 1999]. Average Brunhes spreading rates decrease from 67 mm/yr at 156.2°E to 36 mm/yr at 152.5°E. (Figure 1), however, the rate at the westernmost spreading segment may be somewhat faster if spreading there initiated after the Brunhes/Matuyama boundary. A recent spreading center reorganization occurred at ~80 ka which synchronously affected the segmentation pattern and morphology of the entire ~500 km long spreading system [*Goodliffe et al.*, 1997]. The active spreading centers and the naming convention used here are shown in Figure 2.

3. Data and processing

Geophysical surveys have mapped the seafloor spreading axis, the current western rifting tip, and much of the flanking seafloor and margins with sidescan sonar and multibeam bathymetric systems (Figure 2) [*Benes et al.*, 1997; *Benes et al.*, 1994; *Crook and Taylor*, 1994; *Deep Ocean Resources Development Co.*, 1995; *Goodliffe et al.*, 1997; *Taylor et al.*, 1995]. Together with older geophysical surveys [*Binns et al.*, 1987; *Binns and Whitford*, 1987; *Taylor*, 1987; *Weissel et al.*, 1982] and satellite altimetry-derived gravity measurements [*Sandwell and Smith*, 1995] (Figure 3), these data provide a synoptic view of the entire basin. The majority of data used in this study are from two cruises conducted in 1993, a HAWAII-MR1 sidescan and geophysical survey on R/V Moana Wave [*Taylor et al.*, 1995] and a Hydrosweep multibeam bathymetry and magnetics survey on R/V Hakurei Maru 2 [*Deep Ocean Resources Development Co. 1995*]. Other surveys used include a 1985 SeaMARC II and geophysical survey of the eastern end of the basin [*Crook and Taylor*, 1994], a 1982 R/V Kana Keoki cruise [*Taylor and Exon*, 1987] and compiled single ship tracks and more widely spaced surveys available through the archives of the National Geophysical Data Center (NGDC) in Boulder, Colorado. A more extensive description of these compiled data is given in *Goodliffe et al*. [1999]. Data processing and display utilized the "GMT" software [*Wessel and Smith*, 1995].

Bathymetry

Swath bathymetry data from the HAWAII MR-1 survey (at 5 nautical mile track spacings) and Hydrosweep surveys (at 2.5 nautical mile track spacings) map the entire Woodlark Spreading Center from the spreading tip near 151°35'E to the last active segment intersecting the Simbo Transform at 156°30'E and eastward to the trench [*Deep Ocean Resources Development Co.*, 1995; *Goodliffe et al.*, 1997]. In mapping the surrounding areas,

wide beam profiler data from NGDC cruises and digitized soundings from Australian Navy charts were incorporated in the data base. Where only sparse shipboard data were available (mainly Coral and Solomon Seas and edges of the eastern Woodlark Basin) data from a world wide 2 arc minute grid of predicted and observed bathymetry values [*Smith and Sandwell*, 1997] were also used. Land topographic data for the Papuan Peninsula and islands surrounding the Woodlark Basin are from the USGS 30 arc second worldwide digital elevation model (GTOPO30). These combined data were median filtered and gridded at 0.01° in latitude and longitude (Figure 2). A more detailed map of the merged HAWAII-MR1 and Hydrosweep swath bathymetry data sets at a higher grid resolution (0.002°) is shown in Figure 4.

Free Air Gravity

Shipboard free-air gravity anomaly data were cross-over adjusted and discrepancies removed on a cruise by cruise basis with respect to a R/V Ewing 1995 crossing of the Woodlark Basin. This cruise was used as a reference because of the high quality of its gravity data (collected with a BGM-3 gravity meter [*Bell and Watts*, 1986]) and navigation (using the Global Positioning System) and because it crosses the entire basin from west to east, intersecting most other cruises. After each cruise with an intersection with the Ewing 1995 data was adjusted, remaining cruises were adjusted by removing the average discrepancy of each of these with respect to the corrected ensemble of the first group. In the case of the R/V Moana Wave 1993 cruise, intermittent problems with the gravimeter created stepped offsets in the gravity data. For this cruise the data were divided into four segments bounded by the offsets and each segment was adjusted individually to remove its average discrepancy with respect to previously adjusted cruise data. The locations of the shipboard data used are shown in Figure 3.

We have also merged satellite altimetry-derived gravity data from *Sandwell and Smith* [1995] with the ship data. The gridded satellite altimetry-derived gravity data were sampled at the location of the adjusted ship data and the average discrepancy was removed from the satellite data. Next, a combined data set was compiled by using the adjusted shipboard measurements and gradual tapering to the satellite-derived values over a distance of approximately 5 nautical miles. This was done to preserve the higher resolution of the ship data [*Neumann et al.*, 1993] while using the uniform but lower resolution satellite coverage to constrain the gravity field between widely spaced ship tracks, primarily in the eastern basin. A map of the combined gridded ship and satellite altimetry-derived free-air gravity data is shown in Figure 3.

Bouguer Gravity Anomalies

Using a 3-dimensional (3-D) Fourier transform method [*Parker*, 1972] and the 0.01° gridded bathymetry, gravity values were forward calculated assuming a density of 2800 kg/m^3 for the topography and 1000 kg/m^3 for seawater. We employ this method rather than a more computationally complex method [*Parker*, 1995] that can treat both subareal and submarine topography because most of our gravity data and our principal interests are in investigating the deep oceanic basins. Because the Fourier method used requires that the observation plane (sea level) be above all the relief, the gridded topographic surface was truncated at a depth of 100 m prior to the calculation. The forward calculated anomalies were then subtracted from the free-air anomalies to produce Bouguer anomalies. These are shown in Figure 5. In parts of the margins where there is significant thickness of sediment the Bouguer correction is overestimated. However, the oceanic parts of the basin have little sediment cover so that the uniform topographic density assumption should be valid here. The Bouguer gravity calculation removes the 3-D gravitational effect of the seafloor topography. Remaining anomalies reflect sub-seafloor density variations and errors in the uniform seafloor density assumed. Among these crustal thickness variations and thermal structure are the most significant.

Isostatic Gravity Anomalies

Airy isostatic crustal thickness were calculated from the topography assuming that seafloor at a depth of 3500 m, corresponding roughly to the average depth of the eastern basin, has a crustal thickness of 6 km. Densities of 1000, 2800, and 3300 kg/m^3 were assumed for sea water, crust, and mantle respectively. Account was taken for subareal and submarine topography in isostatically locating the Moho. Crustal thicknesses calculated by subtracting the isostatically located Moho grid from the topographic grid and smoothing to remove excessive short-wavelength variations are shown in Figure 6.

The gravity effects associated with the Moho variations were calculated using the 3-D

Fourier method [*Parker*, 1972] and removed from the Bouguer anomaly to produce the isostatic gravity anomaly map shown in Figure 7. If the isostatic model produces small residual anomalies then the predicted crustal thickness variations can be considered consistent with both topographic and gravity constraints. Other causes of topographic variations, however, such as thermal structure or dynamic effects are not distinguished by this model. Because of this we use the isostatic model to investigate an end-member case in which topographic variations are ascribed to crustal thickness differences between the basins. An alternative end-member in which the topographic differences are ascribed to thermal effects is developed and discussed in a later section.

Because the above calculations are based on local isostasy they do not include effects due to possible slab remnants at the Trobriand and Pocklington Troughs. The deep trenches thus cannot be modeled using the simple local isostatic assumption because of loads that are not described by the topography. Similarly, sediment thickness variations on the rifted margins are not sufficiently well known to take their effect into account. Thus unaccounted for effects exist for the Solomon and Coral seas and parts of the margins but should not significantly affect the interior of the Woodlark Basin.

Magnetics

The primary magnetics data are from the 1993 R/V Moana Wave [*Goodliffe et al.* 1999] and R/V Hakurei Maru 2 surveys [*Deep Ocean Resources Development Co. 1995*] collected with proton precession magnetometers. These surveys were run on N-S tracks spaced at 5 nautical miles for the Moana Wave and 2.5 nautical miles for the Hakurei Maru 2 surveys. Figure 8 shows the N-S magnetic profiles from these two surveys but with only the N-bound tracks from the Hakurei Maru 2 survey shown for clarity. Additional ship magnetics data, indicated with dots in Figure 8, were also used in the data compilation but their profiles are not shown for clarity. The shipboard magnetics data and bathymetry were gridded at 0.01° and used to derive a solution for the intensity of magnetization of the seafloor [*Goodliffe*, 1998, *Goodliffe et al.* 1999] following the technique of *Macdonald et al.* [1980]. The magnetization inversion assumes a 1 km thick source layer which conforms to the seafloor. As this solution produced a reversal pattern in qualitative agreement with that from the total field anomalies no annihilator [*Parker and Huestis*, 1974] was added to the solution. The magnetization solution is presented in *Goodliffe et al.* [1999] and *Taylor et al* [1999].

4. Results

Figure 9 summarizes the geophysical variations measured along the current spreading axis and averaged within the basin in 0.01° longitudinal bins. We have calculated the averaged variations from subsets of the gridded data files that lie both within the areas identified as oceanic crust [*Taylor et al.*, 1999] (indicated by a bold line in Figure 9a) and within the swath coverage (shown in Figure 4). In order to minimize the contribution of dynamic effects near the axis of the spreading centers we have excluded values from within 10 km of the present axis from the oceanic basin averages of segments 2-5b, however, all of the oceanic area for segment 1 is included in the averages due to the limited extent of off axis accreted seafloor there. Since the oceanic seafloor narrows and eventually pinches out to the west it is not possible to compare equivalent areas everywhere along the strike of the basin. The areas and ages of the oceanic basins covered by swath bathymetry for segments 2-4 are similar, and we primarily base our comparisons on these areas. The averages for these areas are shown as heavy solid lines in Figure 8. Because of complications involving spreading center jumps to different extents off axis in the different basins [*Goodliffe et al.*, 1997] however we only investigate the first order variations given by the simple longitudinal averages.

Axial and Basin Depth

Figure 9b (fine line) shows depths along the Woodlark Basin spreading axis. Axial depths fall into two distinct groups. West of the Moresby Transform ridge axis depths are ~2400-3000 m. To the east, depths are ~3400-4000 m. Exceptions include axial depths near the large offset between segments 1c and 2 where the segment ends deepen to about 3500 m and at Cheshire Seamount [*Binns et al.*, 1987] near the eastern end of segment 1a which shallows to ~1750 m. Segment 1a does not have a distinct ridge-like morphology and its neovolcanic zone is dominated by the ~8 km diameter Cheshire Seamount and a low-relief caldera to its west. Within the high backscatter neovolcanic zone small volcanic cones are discernible in the sidescan imagery [*Taylor et al.*, 1995], but no well-defined abyssal hill fabric is evident in the HAWAII-MR1 imagery or bathymetry. The axis of segment 2 is significantly higher than the surrounding seafloor (~300 m), forming a rifted high near its

center which becomes deeper toward the segment ends. Average flank depths for segment 2 (Figure 9b, heavy line) form a flatter profile than the humped along axis depths. These features suggest the axial depth variations include dynamic effects which disappear off axis, as at fast spreading mid-ocean ridges [*Madsen et al.*, 1984]. In the eastern basin, the average and axial profiles are more discordant in shape due to the greater change in segmentation pattern between the pre- and post-reorganization axis. Axial depths are typically 300-500 m deeper than the flanks, forming 10-20 km wide axial valleys. Eastern basin average flank depths are systematically deeper by about 500 m than western basin averages surrounding segment 2 and axial depths are nearly 1 km deeper. Moresby Transform has a maximum depth of ~4700 m recorded in HAWAII-MR1 bathymetry data.

Oceanic Seafloor Texture

Figure 4 shows the swath coverage of the Woodlark Basin. The shading simulates illumination from the north and highlights seafloor texture. Areas outside the swath coverage are shown colored but without shading. The pre-reorientation spreading fabric has a nearly E-W trend in both basins, indicating a consistent almost N-S spreading direction. The swath coverage near Moresby Transform spans the seafloor spreading development from the continental margins to the axis for both basins. It shows that the contrasts in depth and texture between the basins initiated at continental breakup and have persisted throughout the subsequent spreading development.

The western basin segment 2 has abyssal hill relief typically 100-200 m in height with slightly higher relief near the Moresby Transform. The older abyssal hills flanking segment 2 trend at an azimuth of 279° and are truncated by the reoriented spreading center, which trends 265°. Segments 1a, 1b, and 1c are difficult to define in the bathymetry and their axes are primarily identified from the high backscatter of their neovolcanic zones [*Taylor et al.*, 1995]. Oceanic seafloor produced by these axes is associated with many small volcanic cones, with closely-spaced abyssal hill-like fabric developed in only a few places.

The eastern basin has rougher seafloor fabric. Typically, the abyssal hills have a relief of 200-400 m and often extend the full length of the pre-reorientation segments. Their relief is generally lower near the center of the pre-reorientation segments and increases toward the fracture zones. Immediately east of Moresby Transform and its extension bordering the Woodlark Rise, the abyssal hills have particularly large relief and are curved inward toward the axis. Inside-corner highs are developed at the segment 3-4 and 4-5 transforms.

Spreading centers offsets

The western spreading centers have non-transform offsets and the flanking seafloor shows no evidence that transforms ever formed in the western basin. Segment 1a appears to have nucleated in an overlapping configuration with the segment to the east. Based on the configuration of the Brunhes boundary it appears that segments 1b and 1c developed an overlapping configuration as a result of the fragmentation of the previous single segment in this area. The segment 1c-2 offset currently has little overlap, although prior to the 80 ka reorganization the spreading centers had an overlap to offset ratio of about 2.

The primary eastern spreading center offsets are formed by transforms. The transforms between segments 3, 4, and 5, have a component of opening since the 80 ka reorganization. A narrow N-S trending fracture zone extends from the segment 3-4 transform to the edges of the swath coverage. The lower resolution profiler and satellite data suggests it continues to near the edges of the basin (Figure 2). The segment 4-5 offset propagated eastward forming pseudofaults with evidence of discrete rotated lithospheric blocks along the northern band of transferred lithosphere (Figure 4). The transform at the eastern end of segment 5 extends to the trench where its intersection forms a triple junction [*Crook and Taylor*, 1994]. The spreading sub-segments that developed after the 80 ka reorientation in the eastern basin lie primarily within the axial valleys of the major segments and appear not to have formed transforms.

Magnetic character of the basin and axes

Weissel et al. [1982] first noted that near-axis magnetic anomaly amplitudes are greater in the western basin than in the eastern basin. This observation is confirmed and further quantified in the more extensive data now available (Figure 8). In the eastern basin root mean square (rms) magnetic field and seafloor magnetization variations are 136 nT and 4.2 A/m respectively whereas in the western basin rms values are 273 nT and 6.6 A/m. Figure 9d shows the axial and average absolute amplitude of the magnetization intensity across the oceanic basins.

High magnetic amplitudes may result from melt fractionation similar to that proposed for oceanic propagating rifts [*Christie and Sinton*, 1981; *Sinton et al.*, 1983]. At the western end of the basin "ferrobasalts" have been reported near the magmatic tip of the spreading center [*Binns and Whitford*, 1987]. The recent nucleation of the westernmost spreading centers and proximity of colder rifted margins may produce an environment similar to that of propagating rift tips. Magnetization inversions [*Goodliffe*, 1998; *Taylor et al.*, 1995], and the values plotted in Figure 9d generally show higher values near the ends of spreading segments compatible with this mechanism for higher fractionation there. However, this mechanism does not explain the generally higher magnetizations within the interior of the western basin away from the ends of the spreading centers.

The magnetizations described above are calculated using a standard model assumption of a constant source layer thickness [*Macdonald et al.*, 1980]. An alternative valid assumption, however, is that the source layer thickness varies and that magnetization intensity remains constant [*Parker and Huestis*, 1974]. The western basin's apparently higher magnetizations are thus also compatible with a thicker source layer there. If a similar intrinsic magnetization strength for the source layer actually pertains for both basins the higher calculated magnetizations in the western basin could represent a ~50% thicker source layer based on an approximately inverse proportionality between modeled magnetization intensity and source layer thickness [*Parker and Huestis*, 1974]. In the case of a thickened oceanic crustal section two mechanisms may contribute to the observed increase in magnetic field strength. Firstly, although the magnetic source layer in the oceanic crust has been modeled to correspond primarily to the extrusives (layer 2A, [*Talwani et al.*, 1971]), other evidence suggests the deeper crust (layer 3) may also have a significant contribution. In-situ drilling measurements and sampling of gabbros near the South West Indian Ridge indicate that layer 3 can retain a significant remanent magnetization estimated to be capable of contributing 25 to 50% of the magnetic signal observed at the sea surface [*Pariso and Johnson*, 1993a, b]. Modeling of anomalous skewness in marine magnetic anomalies also suggests that the lower crust may contribute to the magnetic signal [*Dyment and Arkani-Hamed*, 1995]. Therefor thickening of the oceanic crust in the western basin, even if primarily involving layer 3 as observed in crustal thickness variations in deep ocean basins [*Mutter and Mutter*, 1993], may nevertheless produce a stronger magnetic signal. A second mechanism for enhancing the magnetic field strength, however, may be through direct thickening of layer 2. At volcanic margins both layers 2 and 3 are reported to be thickened (although layer 3 variations make up most of the anomalous thickness) [*Mutter et al.*, 1988; *Zehnder et al.*, 1990]. Thus, an overall increase in crustal thickness with contributions to the magnetic field from thickened layers 2 and 3 are plausible explanations for the greater magnetic amplitudes of the western basin. Alternative explanations involving higher intrinsic magnetizations would require significant geochemical differences between the basins and would not account for the changes in bathymetry and gravity.

Gravity characteristics

Segment 2 in the western basin has an axial free-air gravity anomaly high (Figures 3 and 9g). Values decrease by 40-50 mGals toward the margins where, in places, they form closed-contour lows (Figure 3). Gravity values increase again over the margins and form complex patterns reflecting the rifted basement. To the west, free air gravity values decrease in segment 1, despite its shallower depth, reflecting the narrow width of oceanic crust and the increasing proximity of thickening continental rifted margin roots. The free air gravity field in the western margins surrounding segment 1 delineates sedimentary basins and the forearc basement high between Woodlark and the Trobriand Islands. In the eastern basin, axial free air gravity values form 10-20 mGal lows relative to the flanks. Off axis in the oceanic basin gravity values are relatively flat but decrease by 10-20 mGals near the margins before increasing again over the margins themselves. 10-20 mGal variations within the off-axis oceanic basin generally form transform parallel trends, however, an oblique band of low values appears to be associated with the eastward propagation of the segment 4-5 offset.

Bouguer gravity anomalies are shown in Figures 5 and 9c. A first order feature of the Bouguer anomalies is a step at Moresby Transform with values in the western basin at least 30 mGals lower than those of the eastern basin (Figures 5 and 9c). An overall gradient with westward-decreasing values is also evident (Figure 9c) crossing both eastern and western basins and becomes distinctly steeper in segment 1. The gradient is 0.07 mGal/km in the

area surrounding segment 2 and 0.1 mGal/km in the area of segments 3 and 4 in the eastern basin. Average Bouguer gravity differences in the oceanic basin flanking segments 2 and 3 are ~40 mGals. In plan view the Bouguer gravity pattern follows the v-shape of the basin. Prominent Bouguer gravity lows are associated with the thicker crust of the Rises and become more negative as they converge toward the Papuan Peninsula.

The western basin spreading centers have no distinct expression in the Bouguer gravity field. Gravity anomalies are relatively flat in the oceanic basin surrounding segment 2. Toward the edges of the basin, Bouguer anomalies do not form closed-contour lows as did the free air gravity anomalies, instead the values form downward gradients to the lows associated with the Rises.

The spreading centers of the eastern basin are associated with small (~10 mGal) but distinct relative Bouguer gravity lows following the axial valleys. Except for Simbo Transform, the Bouguer anomalies do not show the distinct transform parallel trends that were evident in the free air anomalies. The triple junction area between Ghizo and Simbo Ridges and the trench is associated with a large (~40 mGal) Bouguer low but other areas at similar distances from the trench have values similar to the rest of the eastern basin. Approaching the New Britain/San Cristobal trench, however, gravity values decrease toward the lows in the area of the Solomon arc. Basin flanking lows associated with the Woodlark and Pocklington Rises are distinctly smaller east of Moresby Transform.

Isostatic crustal thickness variations and gravity anomalies

Isostatic crustal thickness variations are shown in Figure 6. Crustal thicknesses associated with the oceanic crust surrounding segment 2 in the western basin are on average almost 2 km greater than in the eastern basin with even thicker values for segment 1 (Figure 9e). Although there are unaccounted for complications (associated with subduction and with local sedimentary basins) in isostatically modeling the margins, the crustal thickness map (Figure 6) shows a significant increase in the crustal thickness of the Rises west of the Moresby Transform.

Isostatic gravity anomalies calculated using these crustal thickness variations are shown in Figure 7 and axial and average values for the oceanic basin are given in Figure 9f. As shown in these figures, the isostatic assumption largely accounts for the remaining gravity anomalies between and within the basins. The map view shows only a slight ~10 mGal increase in the western basin from the center of the basin toward the margins. The large Bouguer gradient associated with the ocean-rifted margin transition is also largely accounted for. The 30 mGal step across the Moresby Transform is eliminated, although a prominent ~10-15 mGal anomaly at the transform itself remains. In the eastern basin small ~10 mGal anomaly lows remains associated with the spreading centers and a 10-15 mGal low which may be associated with a pseudofault trends NW from segment 5.

Lithospheric thermal model

An alternative to crustal thickness variations for explaining the overall depth and gravity differences between the basins is that they are due to lithospheric or deeper thermal anomalies. A simple one dimensional estimate of the lithospheric thermal structures needed to balance the overall basin depth differences (500 m) can be made by approximating the geotherms by linear gradients (Figure 10). We use thermal parameters from *Parsons and Sclater* [1977] and assume equal crustal thicknesses (6 km) in both basins, a linear gradient between 0°C at the seafloor and 1333°C at the base of the lithosphere, and constant asthenospheric temperatures at greater depth. We vary the equilibrium thickness of the thermal lithosphere similar to the parameterization of *McKenzie* [1978] while maintaining the same crustal structure. Calculated thermal thicknesses that isostatically balance the depth differences are large. In the limiting case, the eastern basin lithosphere must be at least ~17 km thick to balance a 0 km thick (ridge axis-like) thermal structure in the western basin. A 25 km thick eastern lithosphere is in balance with a 9.2 km thick western lithosphere.

Another measure of the differences in thermal structure is obtained by relating the depth differences to models of seafloor thermal subsidence with age (e.g. *Parsons and Sclater* [1977]). The smallest age difference that corresponds to 500 m of subsidence occurs between the axis itself (at zero age) and ~2 Ma flanking seafloor. Off axis, increasingly greater age differences are required because of the square root of age proportionality of this relationship. For example, 500 m of depth difference also corresponds to seafloor ages of 1 and 5.9 Ma.

The above models assume that the mantle at depth in both basins has the same temperature but that the geotherms in the lithospheres are different. We can alternatively

attribute an isostatic depth difference solely to different temperatures in the deep mantle. If we assume the temperature in the deep eastern basin mantle is a nominal 1333°C, then a 102°C higher temperature within a 100 km thick mantle column in the western basin will balance the 500 m depth difference. Proportionally higher temperatures are required for thinner anomalous mantle thicknesses.

These one-dimensional lithospheric thermal structures also predict ~38 mGal higher Bouguer anomaly in the eastern basin that is entirely due to the reduction density used in the slab which replaces the excess thickness of water of the eastern basin. Assuming that the eastern basin has a "normal" thermal structure these examples indicate that without crustal thickness variations, large lithospheric thermal anomalies (approaching average values that are ridge axis-like) or high anomalous deep mantle temperatures are required to explain the shallower depth of the western basin.

5. Discussion

Axial morphology and seafloor texture generally vary systematically with spreading rate at mid-ocean ridges. Slow spreading mid-ocean ridges (10-50 mm/yr) have prominent axial valleys 1.5-3 km deep; at intermediate rates (50-90 mm/yr) the axis has the form of a rifted high; at fast rates (>90 mm/yr) the axis forms a triangular high [*Macdonald*, 1982]. Correspondingly, the amplitude of abyssal hill relief on ridge flanks decreases with increasing spreading rate [*Malinverno*, 1991; *Small*, 1994]. The nature of spreading center offsets also appears to vary with spreading rate. Although non-transform offsets occur on both slow [*Grindlay et al.*, 1991] and fast [*Macdonald et al.*, 1984] spreading centers, very fast spreading mid-ocean ridges appear to have exclusively non-transform offsets [*Naar and Hey*, 1989]. At very fast spreading rates it is believed that the oceanic lithosphere is too thin and weak to maintain discrete transform offsets [*Macdonald*, 1982] even for large (~100 km) offsets [*Martínez et al.*, 1997].

Transitions in spreading center morphology and geophysical characteristics occur abruptly and appear to be step-like, taking place rapidly over a limited range in spreading rate [*Malinverno*, 1993; *Small and Sandwell*, 1989]. Changes in off-axis seafloor roughness are also step-like and associated with axial morphology changes [*Ma and Cochran*, 1996]. Although these changes are generally correlated with spreading rate, studies suggest they are more fundamentally linked to properties such as thermal structure, crustal thickness, and occurrence and depth of a magma chamber [*Carbotte et al.*, 1998; *Chen and Morgan*, 1990; *Ma and Cochran*, 1996; *Small and Sandwell*, 1989]. The anomalous characteristics of the Reykjanes Ridge [*Bell and Buck*, 1992], the Southeast Indian Ridge near the Australian Antarctic discordance [*Cochran et al.*, 1995; *Sempéré and Cochran*, 1996], and the occurrence of a large non-transform offset at the slow spreading mid-ocean ridge over the Icelandic hotspot [*Macdonald et al.*, 1984] illustrate that spreading rate alone is not the fundamental control on spreading center characteristics.

The Woodlark Basin exhibits abrupt changes in geophysical and morphologic characteristics that are similar to intermediate to fast spreading rate transitions but are in an opposite sense to observed spreading rate variations. Although there is increasing ocean basin maturity from west to east, the characteristics of each basin have been consistently different from their inception. The available data from near the edges of the basins show, for example, that the eastern basin did not exhibit "fast-spreading" characteristics in its earlier history and thus the present observed contrasts do not represent developmental stages in the Woodlark basin.

Below we discuss and evaluate alternative explanations for the differences between the basins. A more definitive examination of these possibilities requires additional information, including systematic sampling to determine the composition of the crust, seismic crustal thickness determinations, and heat flow measurements. Since the available data of these types are only of a reconnaissance nature or absent, the following evaluation is tentative, but based on general observations from the Woodlark Basin and elsewhere.

Mantle Thermal Anomaly

Although locally higher temperatures in the mantle may appear to be the simplest explanation for the differences between the basins, there are several problems with this mechanism. The abrupt step-like change in properties across the basins suggests that such an anomaly would have to be small and shallow since it is confined to the western basin at Moresby Transform, a lithospheric feature. It is difficult to explain how such a small isolated thermal anomaly would form and be maintained since thermal conduction should dissipate it in a relatively short time.

Larger, deep mantle temperature anomalies such as from plumes or hotspots have influences over broad areas which generally cross fairly large offset (~100 km) transforms even when the hotspot is off axis [*Ito et al.*, 1997]. One explanation for this is that plume material is channeled in a low viscosity zone below the lithosphere [*Schilling*, 1991]. Another difficulty with a plume model is that it would have to coincidentally begin its influence on the development of the western oceanic basin precisely at continental breakup, as the margins show no indication of excessive rift-stage volcanism. In particular, models of plume flow [*Ito et al.*, 1997; *Schilling*, 1991] predict that hot upwelling mantle can be channeled by the sloping geometry of the base of the lithosphere. Since the eastern basin evolved earlier it represented thinner lithosphere until breakup in the western basin. Upwelling plume material beneath the western basin would have been channeled to the eastern basin if it arrived before breakup in the western basin. Although not well resolved in available geoid data (combined Seasat and Geosat data by William Haxby, unpublished compilation, 1988), there appears to be no discernible geoid step between the basins that would indicate a deep source beneath one side.

Another source of local thermal anomalies is subduction. Although both eastern and western margins were affected by Paleogene Coral Sea subduction, thermal effects related to subduction should be most pronounced in the western basin where more recent and continuing slow subduction may be active at the Trobriand Trough [*Davies et al.*, 1984]. Although shear strain heating has been suggested as a local consequence of subduction [*Oxburgh and Turcotte*, 1971], seismic and other results indicate that the primary thermal effect of subduction is to cool the surrounding mantle [*Anderson*, 1998]. For example, the cooling effect of the subducting slab has been invoked to explain the slow-spreading characteristics of the East Scotia backarc basin despite its intermediate spreading rates [*Livermore et al.*, 1997]. Subduction at the Trobriand Trough therefore would predict a cooler mantle environment and slower-spreading characteristics in the western basin, opposite to what is observed. Compositional effects that may be related to subduction in the context of a backarc environment are discussed in a later section.

Thermal effects associated with Paleogene crustal underthrusting at the western Pocklington Rise [*Rogerson et al.*, 1987; *Weissel and Watts*, 1979], or possible related compressional crustal thickening are complex. Models generally treat a one-dimensional thermal case appropriate to a cratonic interior, rather than relatively narrow orogenic belts such as the proto-Woodlark/Pocklington Rise. An initial lowering of the lithospheric geothermal gradient is predicted by general models of thrusting or collisional crustal thickening [*England and Thompson*, 1986; *Glazner and Bartley*, 1985; *Murrell*, 1986]. One-dimensional modeling indicates that due to crustal heat production the geotherm within the thickened crust will increase relatively quickly and may, for a while, achieve a level higher than its previous equilibrium level [*Glazner and Bartley*, 1985]. Although these models do not specifically treat the effects on the sub-crustal lithosphere, low heat production there suggests that the geotherm in the thickened mantle lithosphere would remain lowered for a significantly longer time and only approach equilibrium by conductive heat transfer from the surrounding asthenosphere. Thus, although continental crustal anatexis may occur through this mechanism, it does not necessarily lead to greater spreading stage melting after continental breakup.

Models of adiabatic decompression melting in an extending continental lithosphere [*Foucher et al.*, 1982; *Furlong and Fountain*, 1986; *McKenzie and Bickle*, 1988] generally predict that if lithosphere is stretched to the same final thickness before breakup, greater quantities of partial melting will result from the extension of a thicker lithosphere because the overall extension factor (β) is greater in this case. Thus, assuming instantaneous stretching and thicker lithosphere resulting in a larger stretching factor in the western Woodlark basin, an initial period of enhanced melting following rifting may be expected. However, as the duration of rifting and thicknesses of continental lithosphere increase so does horizontal conductive cooling, to the extent that melting may diminish or even be prevented [*Alvarez et al.*, 1984; *Bown and White*, 1995; *Pedersen and Ro*, 1992]. Seafloor spreading has been taking place in the easternmost Woodlark basin for at least 6 Ma, but the earlier rift phase of opening is poorly known. Regionally, the onset of tectonic rifting appears to have been synchronous along the length of the system and is dated at 6 to possibly ~8 Ma [*Taylor et al.*, 1999]. Numerical models of passive rifting indicate that significant horizontal heat loss (sufficient to inhibit melting) is expected for rifting times as short as ~10 Ma [*Alvarez et al.*,

1984]. The westward slowing opening rates, longer syn-rift history, and thicker lithosphere would therefore oppose enhanced melting that may be expected due to a greater stretching factor.

Although geochemical samples are few, the available evidence indicates no significant differences in the degree of partial melting in erupted basalts between eastern and western basins. *Klein and Langmuir* [1987] have used the value of Na_2O corrected for the effects of fractionation to 8 wt % MgO of basalts ($Na_{8.0}$) as an indicator of the extent of mantle melting. Na_2O behaves as a moderately incompatible trace element showing highest concentrations at smallest extents of melting. Using this parameter, the initial seafloor spreading basalts near the western tip of the spreading center (dredge D3 from the East Basin, just east of Moresby Seamount [*Binns et al.*, 1987; *Binns and Whitford*, 1987]) have $Na_{8.0}$= 3.1. Eastern Woodlark basin dredges [*Perfit et al.*, 1987] have a $Na_{8.0}$ value of 2.96 [*Klein and Langmuir*, 1987]. Both eastern and western basin $Na_{8.0}$ values are similar and on the global trend of $Na_{8.0}$ vs depth of *Klein and Langmuir* [1987] plot near the high end correlating with ridge axis depths of about 4000 m and indicating relatively low extents of melting.

Mantle compositional effects

All parts of the Woodlark basin have potentially been influenced by subduction events that may have introduced varying compositional heterogeneities into the mantle thereby potentially influencing the subsequent spreading characteristics. Expected effects of subduction on seafloor spreading may be assessed by examining the range of backarc basin characteristics. Slow to intermediate opening rate backarc basins such as those of the Philippine Sea and East Scotia sea have basin depths that are deeper than global mid-ocean age/depth averages [*Park et al.*, 1990]. Seismic refraction results from the Philippine sea also indicate that backarc basins there have thinner crust than in the Pacific but that additional effects possibly related to slab cooling of the deeper mantle may be required to explain the anomalous depths [*Louden*, 1980]. Fast opening backarc basins such as Lau, N. Fiji and Manus have basins that are shallower than mid-ocean age-depth averages [*Park et al.*, 1990]. Although there is as yet no completely consistent generalization regarding the effect of the backarc environment on spreading characteristics, spreading rate trends from backarc basins are in the same sense as those of mid-ocean ridges but opposite to that observed in the Woodlark basin. For slow-opening rates such as in the western Woodlark basin, if a backarc tectonic setting is applicable, it would thus predict a deeper than normal basin.

The direct effect of changing geochemical crustal composition may perhaps be gauged in the eastern Woodlark basin which displays geochemical variations from MORB-like to arc-like. Dredges from the eastern Woodlark basin have been interpreted as indicating an overall gradient in geochemical compositions from normal MORB at > 200 km from the New Britain/San Cristobal trench to significant arc geochemical compositions within 100 km of the trench [*Perfit et al.*, 1987]. It has been proposed that this geochemical gradient may be due to the earlier history of SW directed subduction of the Pacific plate beneath the Solomon Islands [*Perfit et al.*, 1987] that ended with Ontong Java collision [*Kroenke*, 1984]. Despite this geochemical gradient the seafloor proximal to the trench (excluding Ghizo and Simbo Ridges which have been interpreted as more recent volcanic/tectonic complications of the triple junction area [*Crook and Taylor*, 1994]) is similar in overall depth and texture to that of the rest of the eastern basin, and is distinct from that of the western basin. Thus, if the proposed geochemical gradient from MORB to arc compositions regionally exists in this part of the eastern basin [*Perfit et al.*, 1987], it does not appear to result in differences in depth and seafloor texture.

Other possible but poorly known effects may have contributed to the differences between the eastern and western basin. The thicker crust of the margins bounding the western basin may have imparted a crustal contamination. Young axial lavas near the western spreading tip include olivine tholeiites as well as FeTi basalts and low- and high-Si andesites with evidence for both mantle heterogeneity and crustal contamination [*Binns and Whitford*, 1987]. Whether there is extensive crustal contamination in the western basin and to what extent this could contribute to differences between the basins is unknown due to lack of systematic sampling. A fuller investigation of the potential influence of crustal contamination must await future sampling.

Rift-induced convection

Stretching and thinning of the lithosphere during rifting is compensated by upwelling of the asthenosphere into the space created. This component of asthenospheric

advection is passive and is simply that required to fill the void created by thinning the lithosphere. The juxtaposition of hot asthenosphere against colder lithosphere, however, creates a convective instability that results in sinking of asthenosphere near the margin roots and upwelling near the center of the rift [*Buck*, 1986; *Keen*, 1985]. The thickness of the lithosphere, the geometry of the lithospheric roots, and the intensity of the thermal gradients produced are important controls on the degree of convection generated [*Mutter et al.*, 1988]. Rift-induced secondary convection is thus shallow in origin, does not require anomalous mantle temperatures, and its intensity is controlled by the geometry of the rifting lithosphere.

In the Woodlark Basin rift-induced convection appears to be a conceptually plausible explanation for the differences between the eastern and western basins because it is consistent with model predictions [*Mutter et al.*, 1988] based on known and inferred differences in rift margin geometry between the basins. The induced convection model as presented in *Mutter et al*. [1998] emphasizes the effect of wide versus narrow margins in controlling the thermal structure and thereby the generation of secondary convection in the mantle. In the case of the Woodlark Basin, however, both eastern and western margins have undergone similar degrees of stretching (~200 km, [Taylor et al 1999]). The principal differences between the Woodlark eastern and western margins is in their tectonic history leading to an inferred thicker and cooler western margin lithosphere. Near the longitude of Moresby Transform an abrupt westward increase in the elevation and width of the rifted continental margins occurs (Figure 2). A simple isostatic calculation predicts an associated significant increase in crustal thickness (Figure 6). Tectonically, this thickening corresponds to the Paleogene underthrusting of continental crust beneath the western part of an arc system that then existed here [*Rogerson et al.*, 1987; *Weissel and Watts*, 1979]. This underthrusting event would have also thickened the lithosphere and cooled it by inserting cooler continental lithosphere that had been near the Earth's surface beneath the arc lithosphere. In contrast, the eastern part of this system remained a comparatively thin arc, which continued to thin and deepen eastward. The present-day eastern rises, which are the rifted remnants of this arc, show this eastward thinning and pinch out before reaching the current New Britain/San Cristobal trench (Figure 2). Once rifting and breakup occurred these contrasting conditions appear favorable for inducing significant convection in the western basin but only weak or no convection in the eastern basin. This model can thus account for the sense of the observed anomalies. Although driven by the cooling and sinking of the asthenosphere near the rifted margin lithospheric roots, the compensating up-flow augments the upwelling near the center of the basin and lateral flow within the basin (Figure 11). This mechanism can create a thicker oceanic crust in the western basin while maintaining relatively low degrees of partial melting because the convective flow advects a greater volume of material through the zone of melt generation rather than increasing the extent of partial melting [*Zehnder et al.*, 1990]. Lateral flow along the base of the lithosphere also offsets conductive cooling, resulting in a thinner lithosphere. A thicker crust and thinner lithosphere are consistent with the shallower seafloor and lower Bouguer anomalies in the western basin. The higher observed magnetic field and calculated magnetizations in the western basin are also consistent with this model assuming the magnetic source layer also increases with increasing crustal thickness. The lower lithospheric strength predicted for the western basin is consistent with the axial high of its segment 2; stronger lithosphere in the eastern basin is consistent with the occurrence of axial valleys there [*Chen and Morgan*, 1990]. Weaker lithosphere in the western basin would also yield smaller throw faults resulting in more subdued abyssal hill fabric compared to the eastern basin. Similarly, the non-transform offsets of the western basin are favored at weak lithosphere whereas transform offsets are more likely at the stronger eastern basin lithosphere.

The induced convection model implies significant control by the rifting process and margin lithosphere on the early evolution of ocean basins. It has also been proposed to be active in rifts prior to breakup [*Buck*, 1986; *Moretti and Chénet*, 1987; *Steckler*, 1985; *Steckler et al.*, 1998]. Induced convection was proposed to explain the end-member differences between volcanic and non-volcanic passive margins [*Mutter et al.*, 1988] and tied explicitly to observed differences in rifted margin geometry [*Mutter et al.*, 1988; *Hopper et al.*, 1992; *Keen and Potter*, 1995]. In these models the excess magmatism created by rift-induced convection partly intrudes and erupts onto rifted continental crust but, although transient in duration, also persists into the seafloor spreading stage where it creates

thickened oceanic crust for several million years. The contrasts in style of seafloor spreading in the Woodlark Basin are consistent with transient secondary mantle convection in the western basin since the oceanic crust there has a maximum age of only ~1.9 Ma, significantly less than estimates of 3-8 m.y. for the life span of the excess spreading stage magmatism at volcanic margins [*Hopper et al.*, 1992; *Kelemen and Holbrook*, 1995]. The excess ~2 km thick magmatism interpreted for the western basin, is significantly smaller than the 20-25 km igneous crustal thicknesses interpreted for some volcanic margins and suggest that induced convection may produce a continuum of effects on seafloor spreading between the end-member cases of volcanic/non-volcanic margins (e.g. [*Mutter*, 1993]) depending on the vigor of the convection induced by the geometry of the rifting lithosphere. The westward shallowing axial depths in the westernmost basin (segments 1a-c) may indicate increasing thickening of oceanic crust as a result of the breakup of westward thickening continental lithosphere and associated greater secondary convection.

6. Summary and Conclusions

The western and eastern parts of the Woodlark Basin across Moresby Transform exhibit contrasting styles of seafloor spreading similar to fast to intermediate/slow spreading rate transitions but opposite in sense to the observed spreading rates. Overall differences in depth and gravity between the basins can be accounted for by a thicker crust and/or thinner lithosphere in the western basin. These effects can also qualitatively account for the sense of the differences in magnetic characteristics, seafloor texture, ridge axis morphology, and nature of spreading center offsets between the basins. Possible causes for these differences including mantle plumes, local thermal anomalies, or subduction related compositional differences have inconsistencies with available data from the area or more general tectonic observations. A model of rift-induced convection, however, appears to be most plausible. In this model, the thicker rifted margin lithosphere bordering the western basin induces mantle convection there whereas thinner lithosphere bordering the eastern basin either does not induce convection or does so to a smaller degree. The increase in flux of asthenosphere passing through the region of partial melt generation increases the volume of melt produced, although not the degree of partial melting, and therefore can increase crustal thickness. The flow along the base of the lithosphere offsets conductive lithospheric cooling, resulting in a thinner lithosphere compared to passive plate spreading. These effects are qualitatively consistent with the faster-spreading characteristics of the western basin, the low extents of melting inferred from available basalt samples, and the abrupt change in characteristics across the Moresby Transform.

Acknowledgments. We thank Garrett Ito for helpful discussions on this work. We also thank previous reviewers of an early version for their comments and Associate Editor Kieth Louden, Roger Buck, and an anonymous reviewer for their comments which improved the paper. SOEST contribution number 4741. HIGP Contribution 1030. This work was funded by NSF-ODP.

References

Alvarez, F., J. Virieux, and X. Le Pichon, Thermal consequences of lithospheric extension over continental margins: the initial stretching phase, *Geophys. J. R. astr. Soc.*, 78, 389-411, 1984.

Anderson, D.L., The scales of mantle convection, *Tectonophysics*, 284, 1-17, 1998.

Bell, R.E., and W.R. Buck, Crustal control of ridge segmentation inferred from observations of the Reykjanes Ridge, *Nature*, 357, 583-586, 1992.

Bell, R.E., and A.B. Watts, Evaluation of the BGM-3 sea gravimeter system on board R/V Conrad, *Geophysics*, 51, 1480–1493, 1986.

Benes, V., N. Bocharova, E. Popov, S.D. Scott, and L. Zonenshain, Geophysical and morpho-tectonic study of the transition between seafloor spreading and continental rifting, western Woodlark Basin, Papua New Guinea, *Mar. Geol.*, 142, 85-98, 1997.

Benes, V., S. Scott, and R.A. Binns, Tectonics of rift propagation into a continental margin: Western Woodlark Basin, Papua New Guinea, *J. Geophys. Res.*, 99, 4439-4455, 1994.

Binns, R.A., S.D. Scott, and PACCLARK Participants, Western Woodlark Basin: Potential analogue setting for volcanogenic massive sulphide deposits, *Proc. Pacific Rim Congress*, 87, 531-535, 1987.

Binns, R.A., and D.J. Whitford, Volcanic rocks from the western Woodlark Basin, Papua New Guinea, *Proc. Pacific Rim Congress*, 87, 525-534, 1987.

Bown, J.W., and R.S. White, Effect of finite extension rate on melt generation at rifted continental margins, *J. Geophys. Res.*, 100, 18,011-18,029, 1995.

Buck, W.R., Small-scale convection induced by passive rifting: the cause for uplift of rift shoulders, *Earth Planet. Sci. Lett.*, 77, 362-372, 1986.

Carbotte, S., C. Mutter, J. Mutter, and G. Ponce-Correa, Influence of magma supply and spreading rate on crustal magma bodies and emplacement of the

extrusive layer: Insights from the East Pacific Rise at lat 16°N, *Geology*, 26, 455-458, 1998.

Chen, Y., and W.J. Morgan, Rift valley/no rift valley transition at mid-ocean ridges, *J. Geophys. Res.*, 95, 17571-17581, 1990.

Christie, D.M., and J.M. Sinton, Evolution of abyssal lavas along propagating segments of the Galapagos spreading center, *Earth Planet. Sci. Lett.*, 56, 321-335, 1981.

Cochran, J.R., C. Small, Y. Ma, and J.-C. Sempere, The Southeast Indian Ridge between 88° and 120°E: Gravity anomalies and crustal accretion at intermediate spreading rates, *EOS, Trans. Am. Geophys. Union*, 76, 529, 1995.

Crook, K.A.W., and B. Taylor, Structure and Quaternery tectonic history of the Woodlark triple junction region, Solomon Islands, *Mar. Geophys. Res.*, 16, 65-89, 1994.

Davies, H.L., P.A. Symonds, and I.D. Ripper, Structure and evolution of the southern Solomon Sea region, BMR Journal of Australian Geology and *Geophysics*, 9, 49-68, 1984.

Deep Ocean Resources Development Co., South Pacific Seafloor Atlas, sheets 10-11, Woodlark Basin, *Jap. int. Coop. Agency/Metal Min. Ag. Jap./S. Pacif. appl. Geosci. Comm.*, Tokyo., 1995.

Dyment, J., and J. Arkani-Hamed, Spreading-rate-dependent magnetization of the oceanic lithosphere inferred from the anomalous skewness of marine magnetic anomalies, *Geophys. J. Int.*, *121*, 789-804, 1995.

England, P.C., and A. Thompson, Some thermal and tectonic models for crustal melting in continental collison zones, in *Collision Tectonics*, edited by M.P. Coward and A.C. Ries, pp. 83-94, Blackwell, Oxford, 1986.

Foucher, J.-P., X.L. Pichon, and J.-C. Sibuet, The ocean-continent transition in the uniform lithospheric stretching model: role of partial melting in the mantle, *Phil. Trans. R. Soc. Lond, Ser. A* 305, 27-43, 1982.

Furlong, K.P., and D.M. Fountain, Continental crustal underplating: Thermal considerations and seismic-petrologic consequences, *J. Geophys. Res.*, 91, 8285-8294, 1986.

Glazner, A.F., and J.M. Bartley, Evolution of lithospheric strength after thrusting, *Geology*, 13, 42-45, 1985.

Goodliffe, A.M., *The Rifting of Continental and Oceanic Lithosphere: Observations from the Woodlark Basin*, Ph. D. thesis, University of Hawaii, Honolulu, 190 pp., 1998.

Goodliffe, A.M., B. Taylor and F. Martinez, Data report: marine geophysical surveys of the Woodlark Basin region, In Taylor, B., P. Huchon, et al., Proc. ODP Init Repts., 180: College Station, TX (Ocean Drilling Program), in press, 1999.

Goodliffe, A.M., B. Taylor, F. Martinez, R. Hey, K. Maeda, and K. Ohono, Spreading center reorientation by synchronous jumping in the Woodlark Basin, *Earth Planet. Sci. Lett.*, 146, 233-242, 1997.

Grindlay, N.R., P.J. Fox, and K.C. MacDonald, Second-order ridge axis discontinuities in the South Atlantic; morphology, structure, and evolution, *Mar. Geophys. Res.*, 13, 21-49, 1991.

Hey, R.N., A new class of "pseudofaults" and their bearing on plate tectonics: a propagating rift model, *Earth Planet. Sci. Lett.*, 37, 321-325, 1977.

Holbrook, W.S., and P.B. Kelemen, Large igneous province on the US Atlantic margin and implications for magmatism during continental breakup, *Nature*, 364, 433-436, 1993.

Holbrook, W.S., G.M. Purdy, J.A. Collins, R.E. Sheridan, D.L. Musser, L. Glover III, M. Talwani, J.I. Ewing, R. Hawman, and S.B. Smithson, Deep velocity structure of rifted continental crust, U. S. Mid-Atlantic margin, from wide-angle reflection/refraction data, *Geophysical Research Letters*, 19, 1699-1702, 1992.

Hopper, J.R., J.C. Mutter, R.L. Larson, C.Z. Mutter, and Northwest Australia Study Group, Magmatism and rift margin evolution: evidence from northwest Australia, *Geology*, 20, 853-857, 1992.

Ito, G., J. Lin, and C.W. Gable, Interaction of mantle plumes and migrating mid-ocean ridges: Implications for the Galapagos plume-ridge system, *J. Geophys. Res.*, 102, 15,403-15,417, 1997.

Karig, D.E., Remnant arcs, Geological Society of America Bulletin, 83, 1057-1068, 1972.

Keen, C.E., The dynamics of rifting: deformation of the lithosphere by active and passive driving forces, *Geophys. J. R. astr. Soc.*, 80, 95-120, 1985.

Keen, C.E., and D.P. Potter, The transition from a volcanic to a nonvolcanic rifted margin off eastern Canada, *Tectonics*, 14, 359-371, 1995.

Kelemen, P.B., and W.S. Holbrook, Origin of thick, high-velocity igneous crust along the U.S. East Coast Margin, *J. Geophys. Res.*, 100, 10,077-10,094, 1995.

Klein, E.M., and C.H. Langmuir, Global correlations of ocean ridge basalt chemistry with axial depth and crustal thickness, *J. Geophys. Res.*, 92, 8089-8115, 1987.

Kroenke, L.W., Cenozoic tectonic development of the southwest Pacific, *U.N. ESCAP. CCOP/SOPAC Tech. Bull.* 6, 126 pp., 1984.

Leg 173 Shipboard Scientific Party, Drilling reveals transition from continental breakup to early magmatic crust, *EOS, Trans. Am. Geophys. Union*, 79, 173, 180-181, 1998.

Livermore, R., A. Cunningham, L. Vanneste, and R. Larter, Subduction influence on magma supply at the East Scotia Ridge, *Earth Planet. Sci. Lett.*, 150, 261-275, 1997.

Louden, K.E., The crustal and lithospheric thicknesses of the Philippine Sea as compared to the Pacific, *Earth Planet. Sci. Lett.*, *50*, 275-288, 1980

Luyendyk, B.P., K.C. Macdonald, and W.B. Bryan, Rifting history of the Woodlark Basin in the Southwest Pacific, *Bull. Geol. Soc. Amer*., 84, 1125-1134, 1973.

Ma, L.Y., and J.R. Cochran, Bathymetric Roughness of the Southeast Indian Ridge: Implications for crustal accretion at intermediate spreading rate mid-ocean ridge, *J. Geophys. Res.*, 102, 17,697-17,711, 1996.

Macdonald, K., J.-C. Sempere, and P.J. Fox, East Pacific Rise from Siqueiros to Orozco Fracture Zones: Along-strike continuity of axial neovolcanic zone and structure and evolution of overlapping spreading centers, *J. Geophys. Res.*, 89, 6049-6069, 1984.

Macdonald, K.C., Mid-ocean ridges: Fine scale tectonic, volcanic and hydrothermal processes within the plate boundary zone, *Ann. Rev. Earth Planet. Sci*., 10, 155-190, 1982.

Macdonald, K.C., S.P. Miller, S.P. Huestis, and F.N. Spiess, Three-Dimensional modeling of a magnetic reversal boundary from inversion of Deep-Tow measurements, *J. Geophys. Res.*, 85, 3670-3680, 1980.

Madsen, J.A., D.W. Forsyth, and R.S. Detrick, A new isostatic model for the East Pacific Rise, *J. Geophys. Res.*, 89, 9997-10015, 1984.

Malinverno, A., Inverse square-root dependence of mid-ocean-ridge flank roughness on spreading rate, *Nature*, 352, 58-60, 1991.

Malinverno, A., Transition between a valley and a high at the axis of mid-ocean ridges, *Geology*, *21*, 639-642, 1993.

Martínez, F., R.N. Hey, and P.D. Johnson, The East Ridge System, 28.5-32°S East Pacific Rise: Implications for Overlapping Spreading Center Development, *Earth Planet. Sci. Lett.*, 151, 13-31, 1997.

McKenzie, D., and M.J. Bickle, The volume and composition of melt generated by extension of the lithosphere, *J. Petrology*., 29, 625-679, 1988.

McKenzie, D.P., Some remarks on the development of sedimentary basins, *Earth Planet. Sci. Lett.*, 40, 25–32, 1978.

Moretti, I., and P.Y. Chénet, The evolution of the Suez rift: a combination of stretching and secondary convection, *Tectonophysics*, *133*, 229-234, 1987.

Murrell, S.A.F., Mecahnics of tectogenesis in plate collision zones, in *Collision Tectonics*, edited by M.P. Coward, and A.C. Ries, pp. 95-111, Blackwell, Oxford, 1986.

Mutter, J.C., Margins declassified, *Nature*, *364*, 393-394, 1993.

Mutter, J.C., W.R. Buck, and C.M. Zehnder, Convective partial melting 1. A model for the formation of thick basaltic sequences during the initiation of spreading, *J. Geophys. Res.*, 93, 1031–1048, 1988.

Mutter, C.Z., and J.C. Mutter, Variations in thickness of layer 3 dominate oceanic crustal structure, *Earth Planet. Sci. Lett.*, *117*, 295-317, 1993.

Mutter, J.C., M. Talwani, and P.L. Stoffa, Origin of seaward-dipping reflectors in oceanic crust off the Norwegian margin by "subaerial sea-floor spreading", *Geology*, 10, 353-357, 1982.

Naar, D.F., and R.N. Hey, Speed limit for oceanic transform faults, *Geology*, 17, 420-422, 1989.

Neumann, G.A., D.W. Forsyth, and D. Sandwell, Comparison of marine gravity from shipboard and high-density satellite altimetry along the Mid-Atlantic Ridge, 30.5°-35.5°S, *Geophys. Res. Lett.*, 20, 1639-1642, 1993.

Oxburgh, E.R., and D.L. Turcotte, Origin of paired metamorphic belts and crustal dilation in island arc regions, *J. Geophys. Res.*, 76, 1315-1327, 1971.

Park, C.-H., K. Tamaki, and K. Kobayashi, Age-depth correlation of the Philippine Sea back-arc basins and other marginal basins in the world, *Tectonophysics*, 181, 351-371, 1990.

Pariso, J.E., and H.P. Johnson, Do layer 3 rocks make a significant contribution to marine magnetic anomalies? In situ magnetization of gabbros at Ocean Drilling Program hole 735B, *J. Geophys. Res*., *98*, 16,033-16,052, 1993a.

Pariso, J.E., and H.P. Johnson, Do lower crustal rocks record reversals of the Earth's magnetic field? Magnetic petrology of oceanic gabbros from Ocean Drilling Program hole 735B, *J. Geophys. Res*., *98*, 16,013-16,032, 1993b.

Parker, R.L., The rapid calculation of potential anomalies, *Geophys. J. Roy. astron. Soc.*, 31, 447–455, 1972.

Parker, R.L., Improved Fourier terrain correction, Part I, *Geophysics*, 60, 1007-1017, 1995.

Parker, R.L., and S.P. Huestis, The inversion of magnetic anomalies in the presence of topography, *J. Geophys. Res.*, 79, 1587-1593, 1974.

Parsons, B., and J.G. Sclater, An analysis of the variation of ocean floor bathymetry and heat flow with age, *J. Geophys. Res.*, 82, 803–827, 1977.

Pedersen, T., and H.E. Ro, Finite duration extension and decompression melting, *Earth Planet. Sci. Lett.*, 113, 15-22, 1992.

Perfit, M.R., C.H. Langmuir, M. Baekisapa, B. Chappell, R.W. Johnson, H. Staudigel, and S.R. Taylor, Geochemistry and petrology of volcanic rocks from the Woodlark basin: Addressing questions of ridge subduction, in *Marine Geology, Geophysics, and Geochemistry of the Woodlark Basin-Solomon Islands*, edited by B. Taylor, and N.F. Exon, pp. 113-154, Circum-Pacific Council for Energy and Mineral Resources, Houston, TX, 1987.

Rogerson, R., D. Hilyard, G. Francis, and E. Finlayson, The foreland thrust belt of Papua New Guinea, *Proc. Pacific Rim Congress*, 87, 579-583, 1987.

Sandwell, D.T., and W.H.F. Smith, world_grav.img.7.2, *The Geological Data Center, Scripps Institution of Oceanography*, La Jolla, CA, 1995.

Schilling, J.-G., Fluxes and excess temperatures of mantle plumes inferred from their interaction with migrating mid-ocean ridges, *Nature*, 352, 397-403, 1991.

Sempéré, J.-C., and J.R. Cochran, The Southeast Indian Ridge between 88°E and 118°E: Variations in crustal accretion at constant spreading rate, *J. Geophys. Res.*, submitted, 1996.

Sinton, J.M., D.S. Wilson, D.M. Christie, R.N. Hey, and J.R. Delaney, Petrologic consequences of rift propagation on oceanic spreading ridges, *Earth Planet. Sci. Lett.*, 62, 193-207, 1983.

Small, C., A global analysis of mid-ocean ridge axial topography, *Geophys. J. Int.*, 116, 64-84, 1994.

Small, C., and D.T. Sandwell, An abrupt change in ridge axis gravity with spreading rate, *J. Geophys. Res.*, 94, 17,383-17,392, 1989.

Smith, W.H.F., and D.T. Sandwell, Global sea floor topography from satellite altimetry and ship depth soundings, *Science*, 277, 1956-1962, 1997.

Steckler, M.S., Uplift and extension at the Gulf of Suez: Indications of induced mantle convection, *Nature*, 317, 135–139, 1985.

Steckler, M.S., S. Feinstein, B.P. Kohn, L.L. Lavier, and M. Eyal, Pattern of mantle thinning from subsidence and heat flow measurements in the Gulf of Suez: Evidence for the rotation of Sinai and along-strike flow from the Red Sea, *Tectonics, 17*, 903-920, 1998.

Talwani, M., C. Windisch, and M. Langseth, Reykjanes ridge crest: a detailed geophysical study, *J. Geophys. Res.*, *76*, 473-517, 1971.

Taylor, B., and N.F. Exon, An investigation of ridge subduction in the Woodlark-Solomons region: Introduction and overview, in *Marine Geology, Geophysics and Geochemistry of the Woodlark Basin - Solomon Islands*, edited by B. Taylor, and N.F. Exon, pp. 1-24, Circum-Pacific Council for Energy and Mineral Resources Earth Science Series, Houston, Texas, 1987.

Taylor, B., A. Goodliffe, and F. Martinez, How continents break up: insights from Papua New Guinea, *J. Geophys. Res.*, in press, 1999.

Taylor, B., A. Goodliffe, F. Martinez, and R.N. Hey, Continental Rifting and Initial Seafloor Spreading in the Woodlark Basin, *Nature*, 374, 534-537, 1995.

Weissel, J.K., B. Taylor, and G.D. Karner, The opening of the Woodlark Basin, subduction of the Woodlark spreading system and the evolution of northern Melanesia since mid-Pliocene time, *Tectonophysics*, 87, 253-277, 1982.

Weissel, J.K., and A.B. Watts, Tectonic evolution of the Coral Sea basin, *J. Geophys. Res.*, 84, 4572-4582, 1979.

Wessel, P., and W.H.F. Smith, New Version of the Generic Mapping Tools Released, *EOS, Trans. Am. Geophys. Union*, 76, 329, 1995.

Zehnder, C.M., J.C. Mutter, and P. Buhl, Deep seismic and geochemical constraints on the *Nature* of rift-induced magmatism during breakup of the North Atlantic, *Tectonophysics*, 173, 545-565, 1990.

Figure Captions

Figure 1) Location map showing tectonic features of the Woodlark Basin and surroundings; DE is D'Entrecasteau Islands; MT is Moresby Transform; ST is Simbo Transform. Small numbers near spreading centers indicate average Brunhes Chron spreading rates in mm/yr.

Figure 2) Bathymetric map showing the location of present-day spreading centers (double line), Moresby Transform (MT), Normamby (N), Tagula (T), Woodlark (W), and Rossel (R) islands. Other tectonic features as in Figure 1. Contour interval is 500m with annotations in km. The continent/ocean transition is shown as a dark solid line where inferred from complete swath bathymetry coverage and closely spaced geophysical profiles and is dashed where inferred from more widely spaced data.

Figure 3) Free air gravity anomaly map compiled from shipboard and satellite altimetry derived values. The location of shipboard data is shown by fine dots. Values are gray shaded and contours at 10 mGal intervals are shown for the principal areas of interest. Tectonic features, land, and ocean-continent boundary as in Figure 2.

Figure 4) Detail of swath bathymetry from merged HAWAII-MR1 and Hydrosweep surveys showing color-coded depths and highlighting seafloor texture by shading the surface as if illuminated from the north. Areas outside swath coverage are colored but not shaded. The HAWAII-MR1 data in this figure extend from 151°E to 154°45'E (top panel) and the Hydrosweep data extend eastward from there (bottom panel). The continuity of features at the join between the data sets at 154°45'E within the eastern basin (bottom panel) shows that at the grid spacing used in these figures (.002°) the differences in texture between the basins are real and are not due to differences in system resolution.

Figure 5) Bouguer anomaly map calculated using a density contrast of 1800 kg/m^3 for the topography which removes most of the short-wavelength gravity anomalies due to seafloor bathymetric features. Contouring at 10 mGal intervals is shown for the principal areas of interest and shading interval is shown in the scale bar. Tectonic features, land, and ocean-continent boundary as in Figure 2.

Figure 6) Airy isostatic crustal thickness map calculated assuming densities of 1000, 2800, and 3300 kg/m^3 for water, crust, and mantle respectively. The calculation also assumes seafloor at a depth of 3500 m has a crustal thickness of 6 km. Contour interval is 1 km. Shading interval highlight differences between the eastern and western oceanic basins. The grid has been filtered using a .09°x.09° averaging window to smooth out short wavelength bathymetric features. Tectonic features, land, and ocean-continent boundary as in Figure 2.

Figure 7) Isostatic gravity anomaly map calculated by subtracting the gravity effect of an Airy Moho interface from the Bouguer anomalies. Contour interval is 10 mGal. Tectonic features, land, and ocean-continent boundary as in Figure 2.

Figure 8) Magnetic anomaly profiles from R/V Moana Wave and R/V Hakurei Maru 2. Magnetic profiles are projected E-W from track, positive areas shaded dark gray. Inset shows amplitude scale. Profiles east of 154.75°E are from Hakurei Maru 2 and only north-bound profiles are shown for clarity. Other data used in magnetic inversion but not shown here are indicated by dots. Light gray shaded areas indicate bathymetry shallower than 2000 m. Black areas are islands. Double line shows present-day spreading centers. Solid line shows the ocean-continent boundary, dashed where inferred. Note increase in oceanic magnetic field amplitude west of Moresby Transform (154.2°E).

Figure 9) (A) Bathymetry map with numbered spreading centers, ocean-continent boundary, 500 m contours and average Brunhes chron spreading rates in mm/yr shown within boxes. (B-G) Geophysical variations plotted against longitude. Axial profiles are shown with a fine line. Basin

averages were calculated in 0.01° longitudinal bins from the respective grids from areas within both the oceanic boundary (excluding the isolated closed contour at 9°50'S, 152°50'E), the swath bathymetry coverage (shown in Figure 3), and excluding data from within 10 km of the axis for segments 2-5b. Averages from comparable areas of the eastern and western basins are shown as a solid heavy line, other values are dashed. Gray vertical line indicates the longitude of Moresby Transform.

Figure 10) One-dimensional lithospheric columns used to isostatically balance average basin depth differences by varying the geotherm. Axes show temperature as a function of depth. Superscripts on variables refer to western (w) and eastern (e) basin values. Densities in the crust, mantle, and asthenosphere are a function of temperature (T) between 0 and 1333°C (Ta) given by $\rho^o(1-T\alpha)$ where ρ^o= 2800 kg/m^3 for the crust and 3300 kg/m^3 for mantle at 0°C and $\alpha = 3.2 \times 10^{-5}$ C$^{\circ -1}$ for crust and mantle. ρ_w is 1000 kg/m^3 for the water layer. Using values for average water depths of the western and eastern basins (h^w_w = 3000 m and h^e_w = 3500 m) and assuming equal crustal thicknesses in both basins (h_c = 6000 m) h^e_l = 25000 m; yields a value for the western basin lithospheric thickness (h^w_l) of 9200 m. For thinner eastern basin lithosphere, a limit is reached at ~17000 m below which the western basin depth cannot be balanced by additionally thinning the lithosphere using these parameters.

Figure 11) Schematic model of rift-induced convection in the Woodlark Basin. A) Western basin's thick rifted continental margins induce downwelling of the adjacent asthenosphere resulting in a secondary basin-wide convection which increases vertical advection near the basin center and sweeps asthenosphere past the base of the lithosphere at a velocity greater than that of plate spreading. Compared to passive plate spreading, a larger volume of mantle flows through the region of partial melt generation creating a thicker crust and offseting conductive cooling resulting in a thinner lithosphere. The resulting basin morphology and geophysical characteristics mimic a faster spreading rate than the actual plate separation rate determined from seafloor magnetic isochrons. B) Eastern basin with thinner rifted margin crust induces weak or no convection. The asthenosphere is driven passively by plate separation producing characteristics consistent with the observed spreading rates.

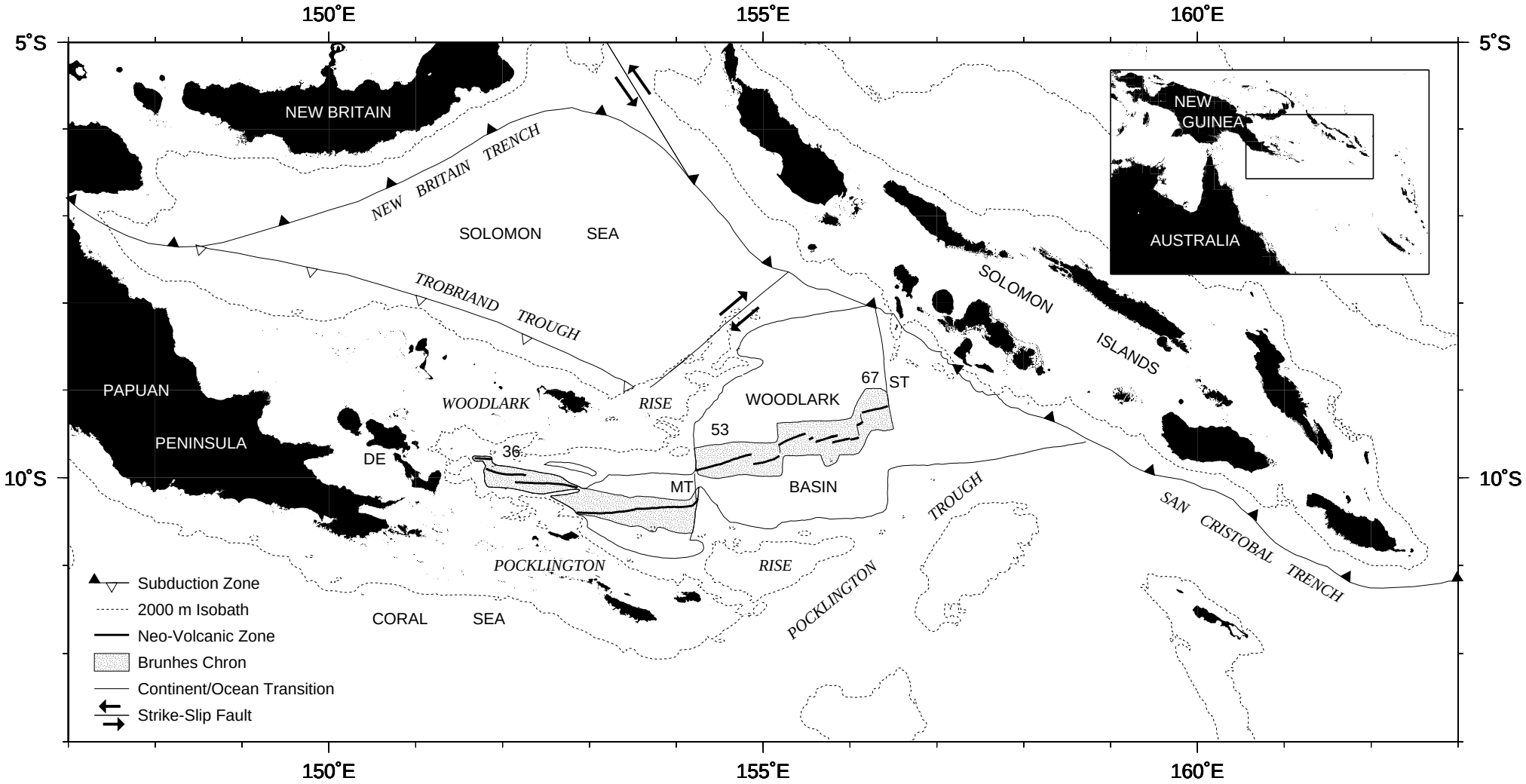
150°E
155°E
160°E
5°S
10°S
NEW BRITAIN
NEW BRITAIN TRENCH
SOLOMON SEA
TROBRIAND TROUGH
PAPUAN
PENINSULA
DE
WOODLARK
RISE
36
53
67
ST
WOODLARK
BASIN
MT
TROUGH
SOLOMON
ISLANDS
SAN CRISTOBAL TRENCH
POCKLINGTON
RISE
POCKLINGTON
CORAL SEA
NEW GUINEA
AUSTRALIA
Subduction Zone
2000 m Isobath
Neo-Volcanic Zone
Brunhes Chron
Continent/Ocean Transition
Strike-Slip Fault

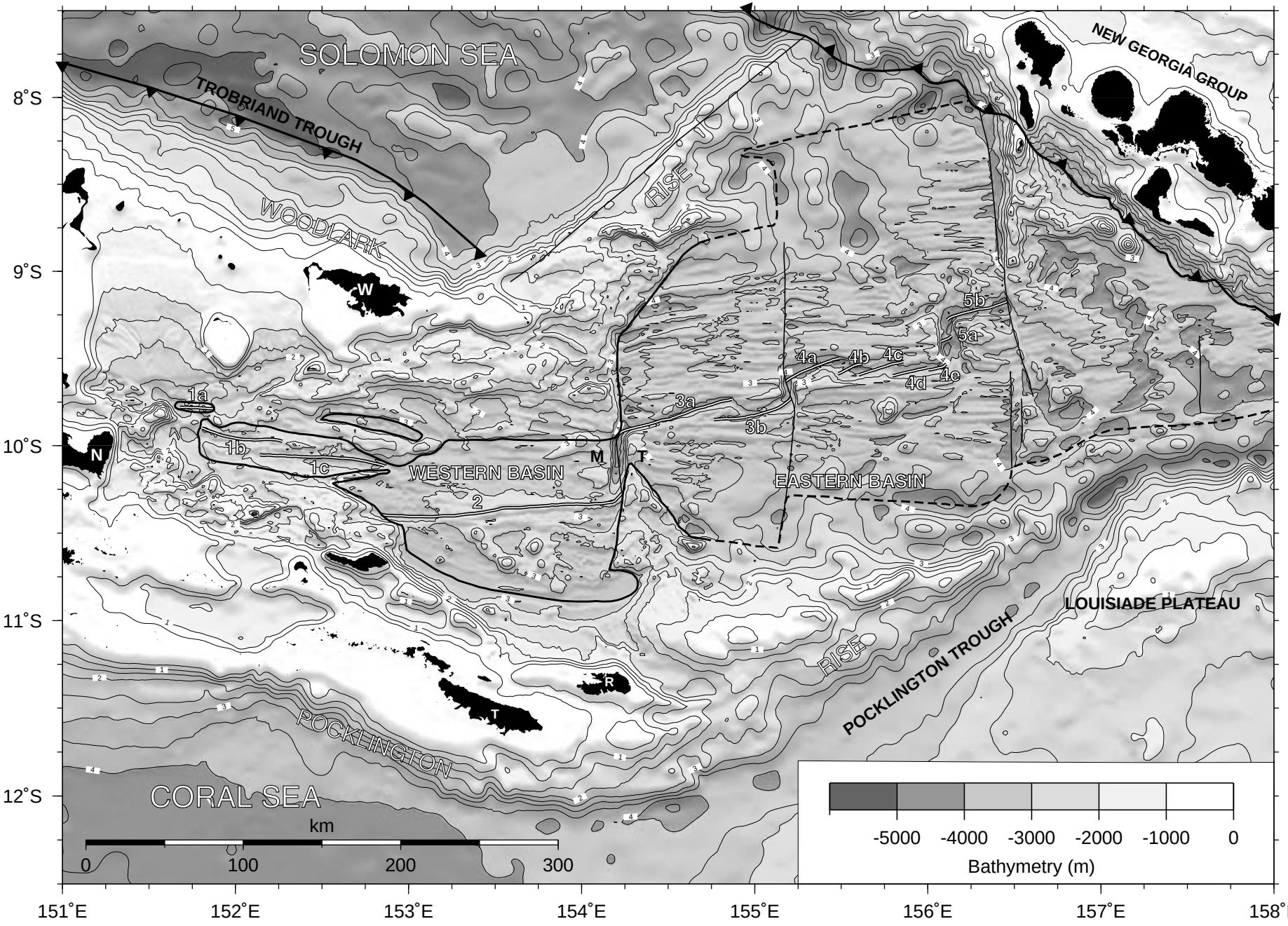
SOLOMON SEA
TROBRIAND TROUGH
WOODLARK
RISE
NEW GEORGIA GROUP
W
N
M
T
R
1a
1b
1c
2
3a
3b
4a
4b
4c
4d
4e
5a
5b
WESTERN BASIN
EASTERN BASIN
LOUISIADE PLATEAU
POCKLINGTON TROUGH
RISE
POCKLINGTON
CORAL SEA
8°S
9°S
10°S
11°S
12°S
151°E
152°E
153°E
154°E
155°E
156°E
157°E
158°E
km
0
100
200
300
-5000
-4000
-3000
-2000
-1000
0
Bathymetry (m)

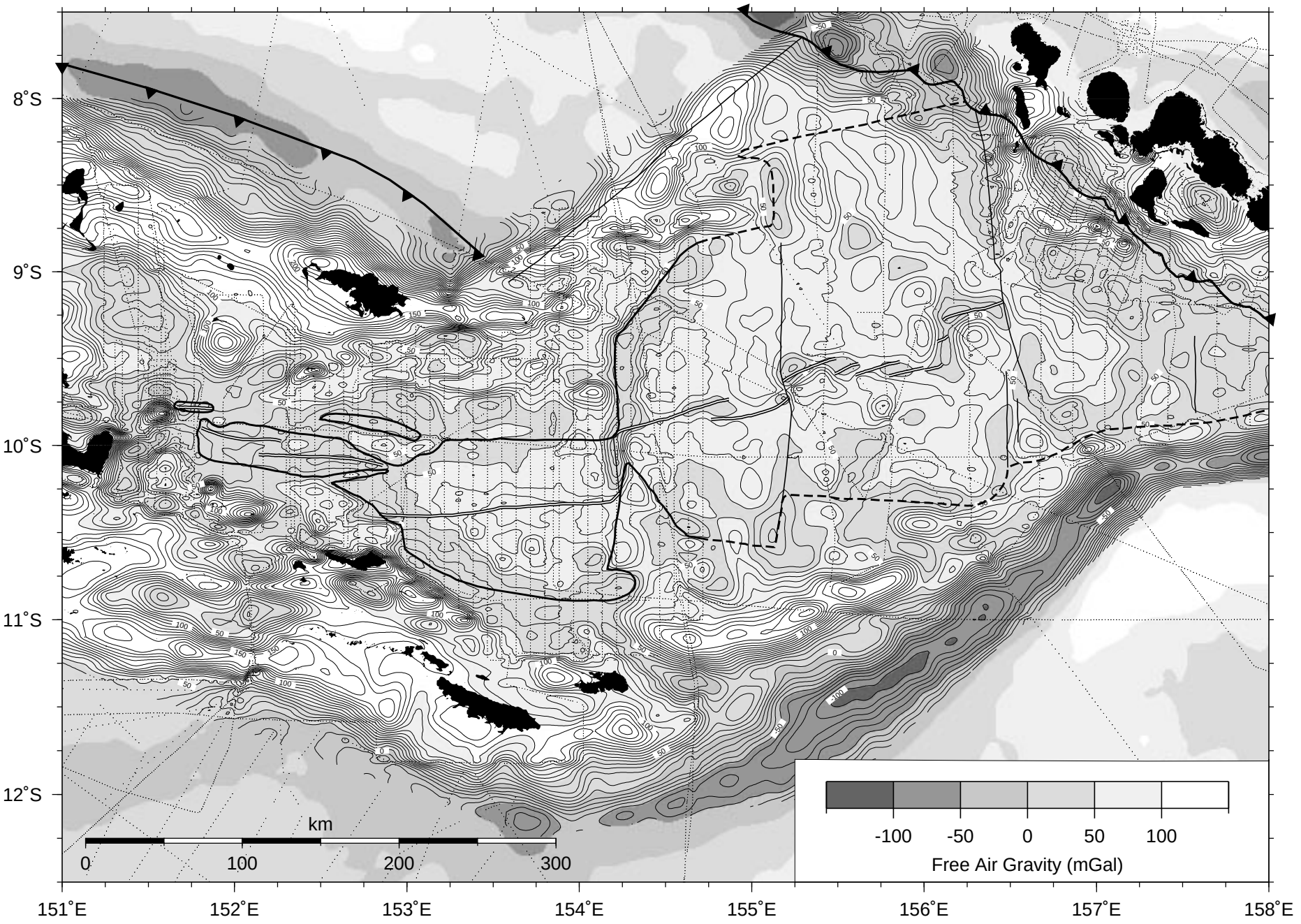
8˚S
9˚S
10˚S
11˚S
12˚S
151˚E
152˚E
153˚E
154˚E
155˚E
156˚E
157˚E
158˚E
km
0
100
200
300
-100
-50
0
50
100
Free Air Gravity (mGal)

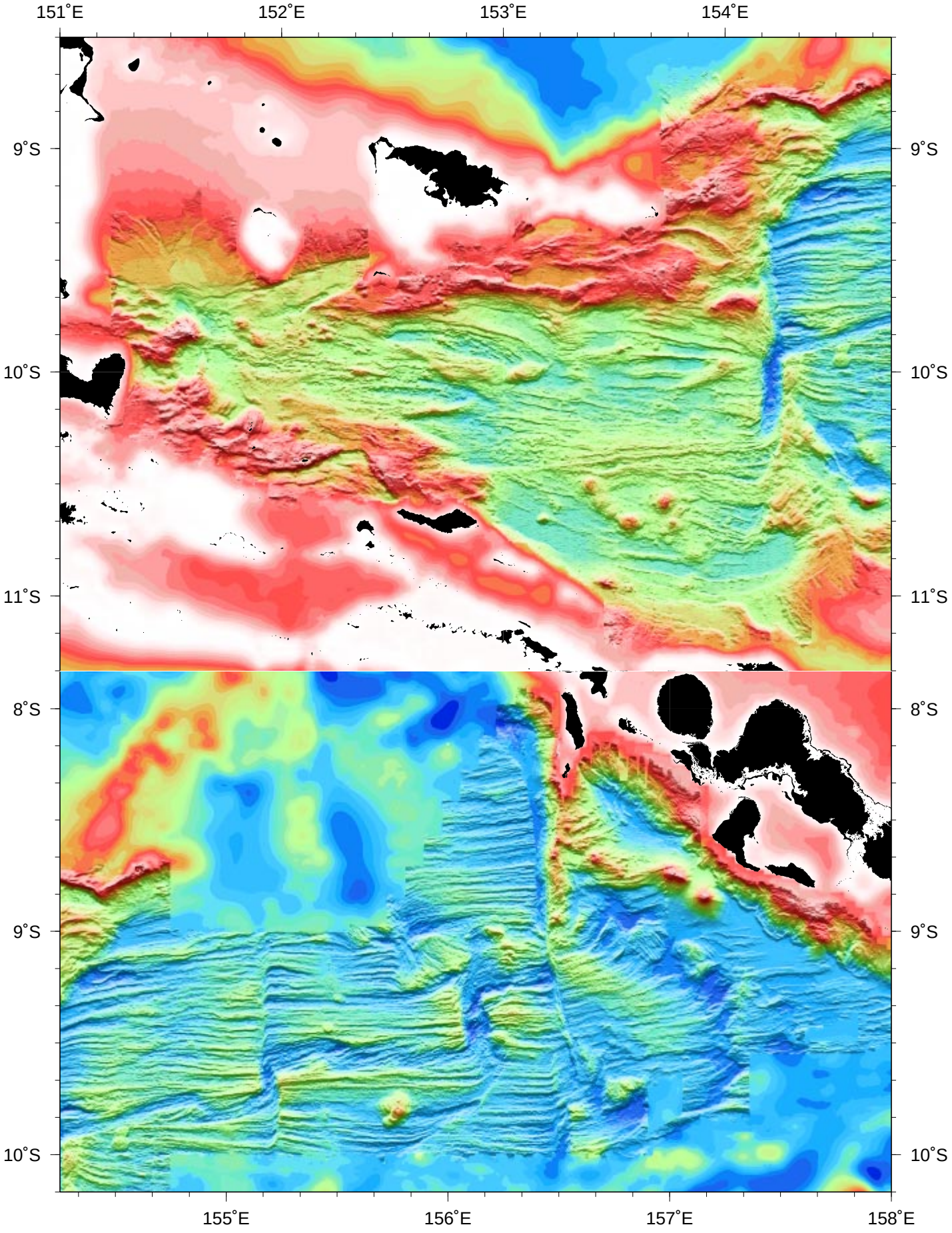
151˚E
152˚E
153˚E
154˚E
9˚S
10˚S
11˚S
8˚S
9˚S
10˚S
155˚E
156˚E
157˚E
158˚E
KM
6 5 4.5 4.2 4 3.8 3.6 3.5 3.4 3.3 3.2 3.1 3 2.8 2.6 2.4 2.2 2 1.8 1.6 1.4 1.2 1 .8 .6 .4 0

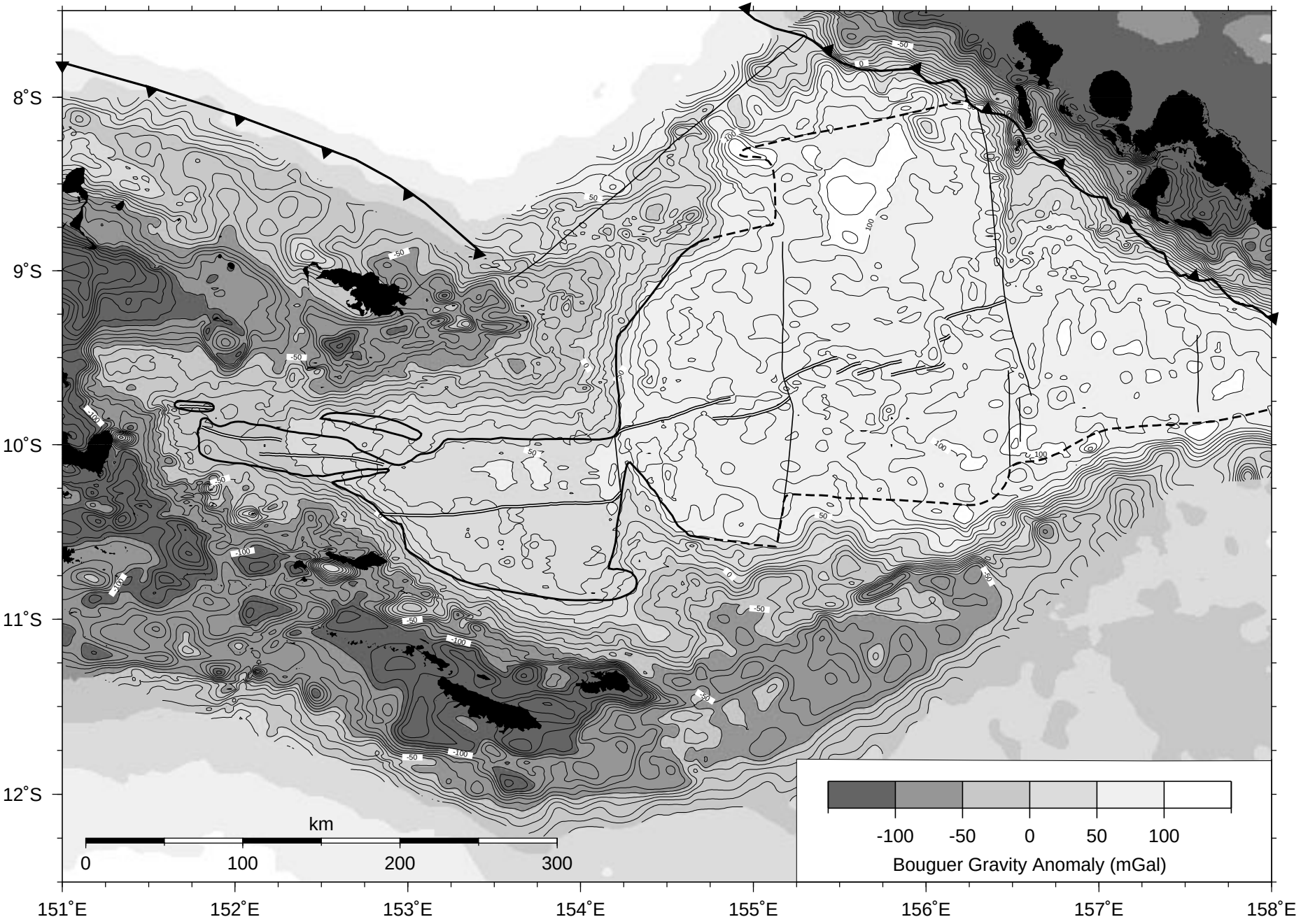
8˚S
9˚S
10˚S
11˚S
12˚S
151˚E
152˚E
153˚E
154˚E
155˚E
156˚E
157˚E
158˚E
km
0
100
200
300
-100
-50
0
50
100
Bouguer Gravity Anomaly (mGal)

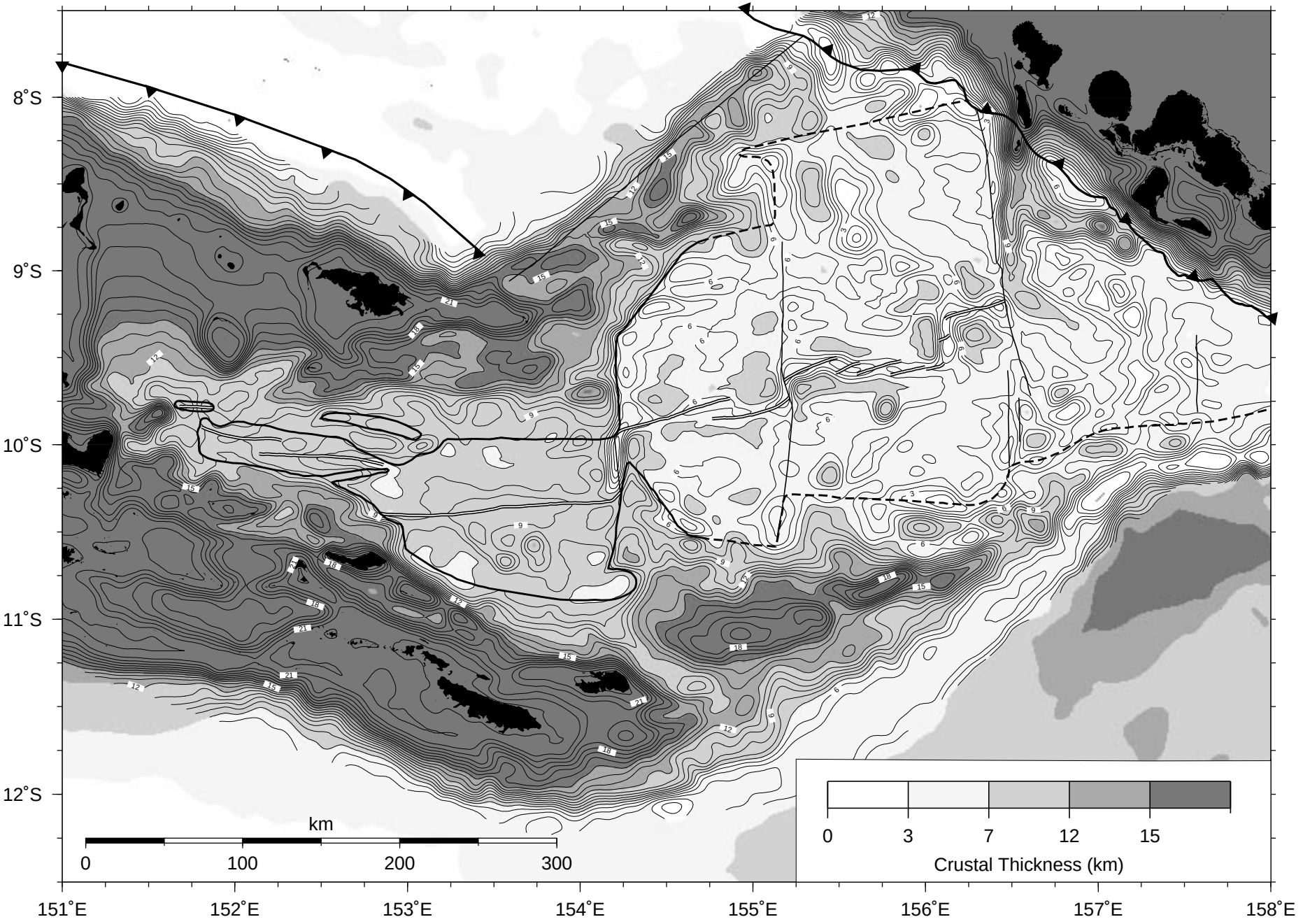
8˚S
9˚S
10˚S
11˚S
12˚S
151˚E
152˚E
153˚E
154˚E
155˚E
156˚E
157˚E
158˚E
km
0
100
200
300
0
3
7
12
15
Crustal Thickness (km)

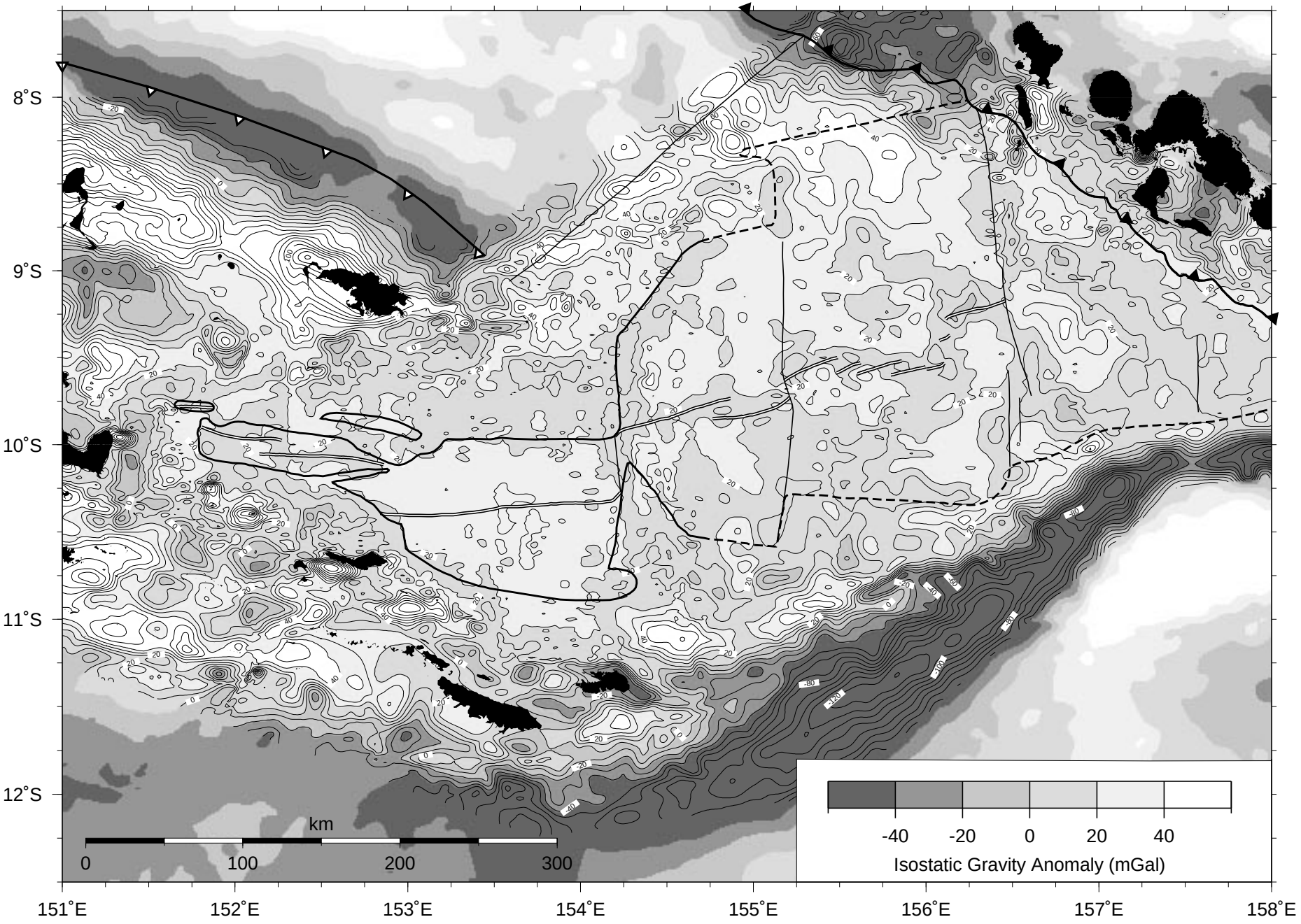
8˚S
9˚S
10˚S
11˚S
12˚S
151˚E
152˚E
153˚E
154˚E
155˚E
156˚E
157˚E
158˚E
km
0
100
200
300
-40
-20
0
20
40
Isostatic Gravity Anomaly (mGal)

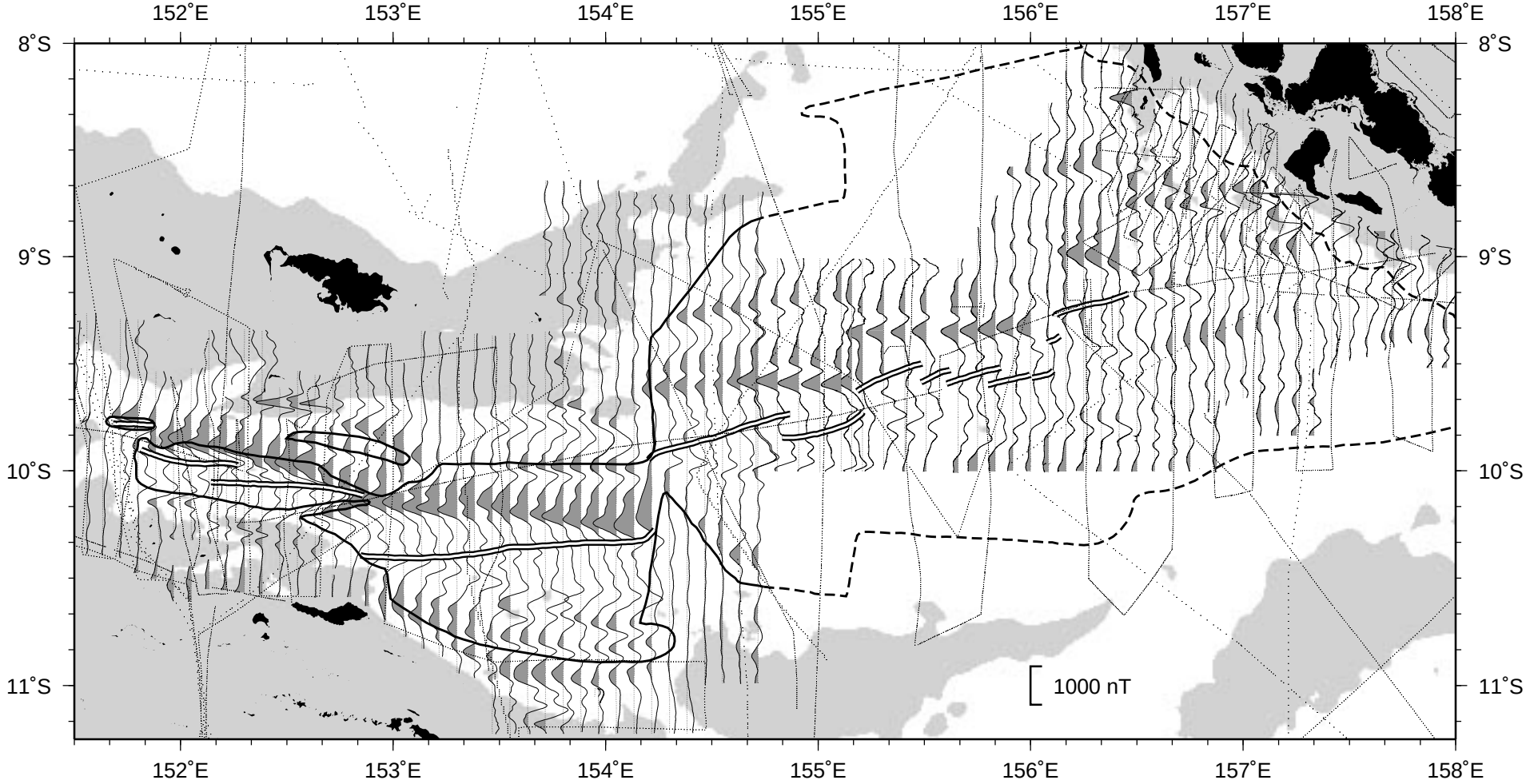
152˚E
153˚E
154˚E
155˚E
156˚E
157˚E
158˚E
8˚S
9˚S
10˚S
11˚S
1000 nT

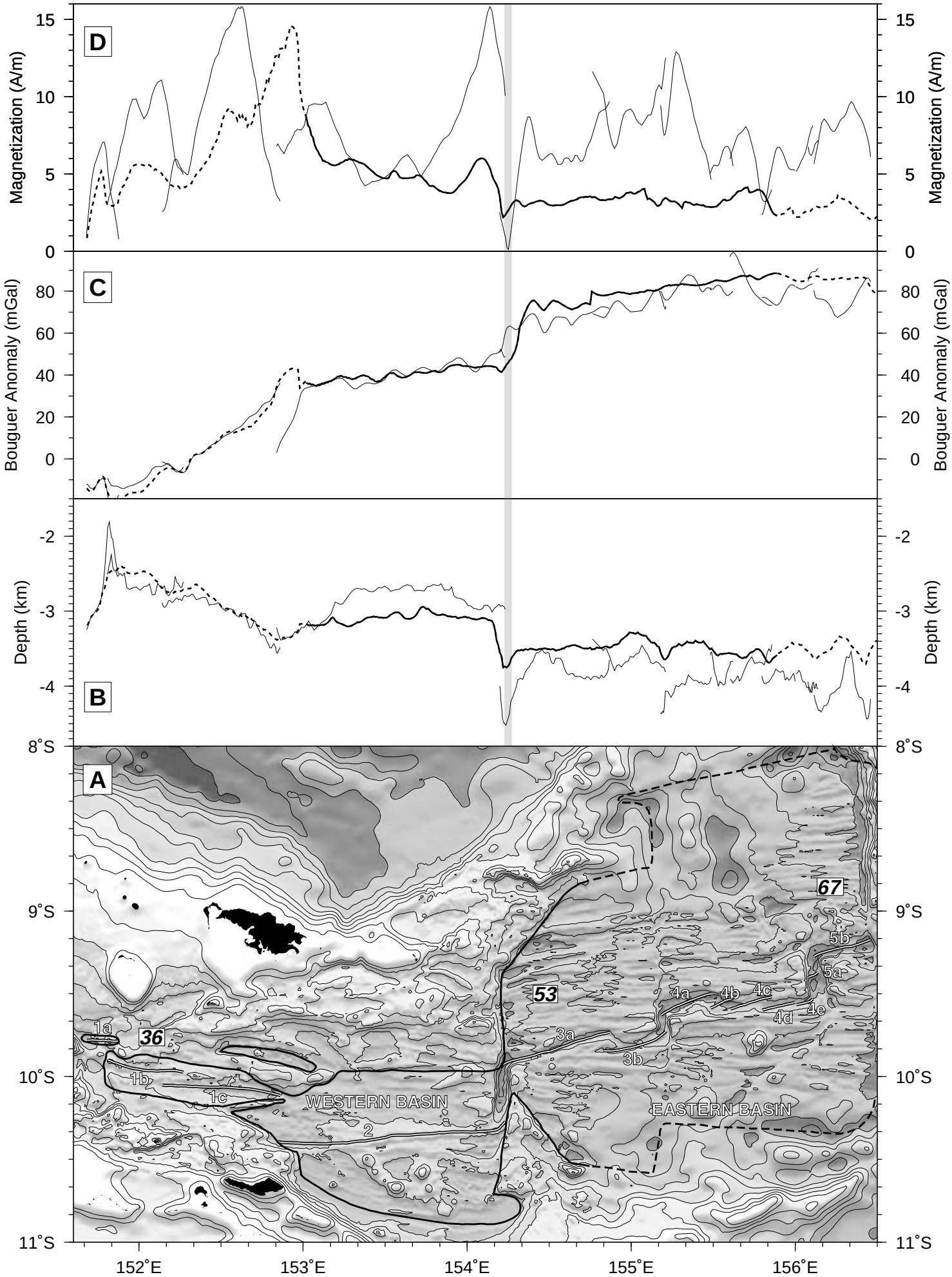
D
Magnetization (A/m)
15
10
5
0
C
Bouguer Anomaly (mGal)
80
60
40
20
0
B
Depth (km)
-2
-3
-4
A
8˚S
9˚S
10˚S
11˚S
152˚E
153˚E
154˚E
155˚E
156˚E
67
53
36
1a
1b
1c
2
3a
3b
4a
4b
4c
4d
4e
5a
5b
WESTERN BASIN
EASTERN BASIN

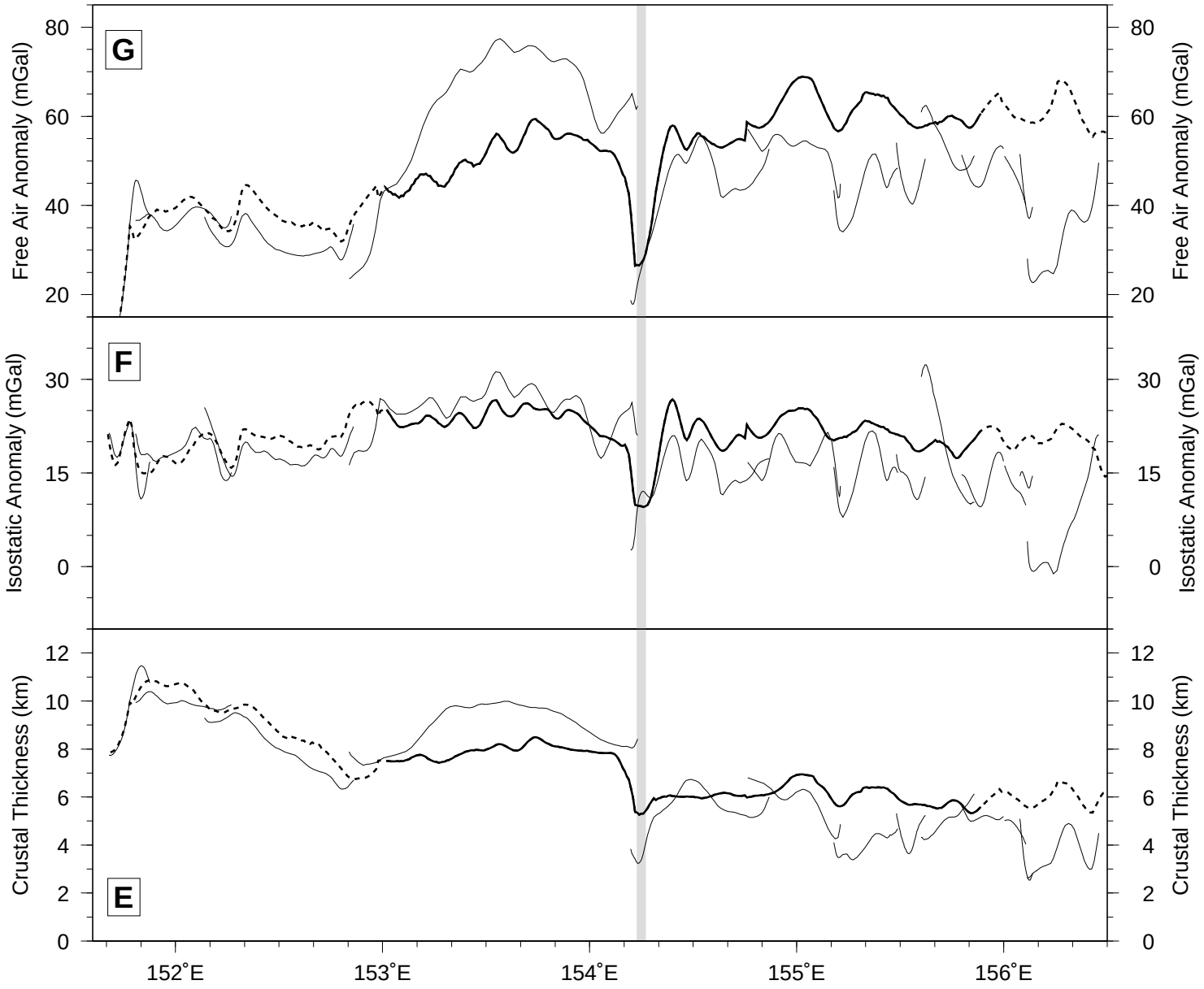
G
F
E
Free Air Anomaly (mGal)
Isostatic Anomaly (mGal)
Crustal Thickness (km)
80
60
40
20
30
15
0
12
10
8
6
4
2
0
152˚E
153˚E
154˚E
155˚E
156˚E

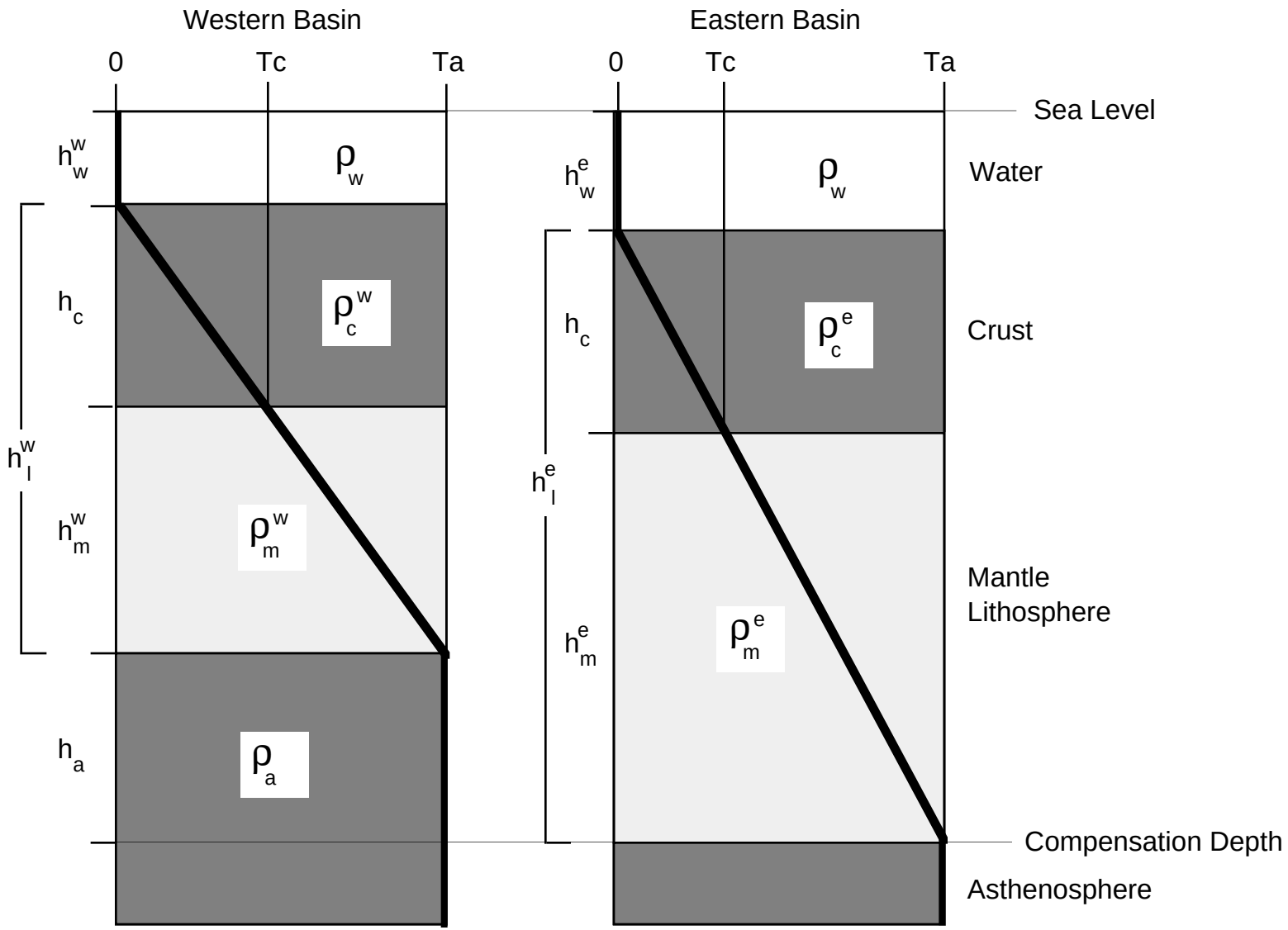
Western Basin
Eastern Basin
0
Tc
Ta
0
Tc
Ta
Sea Level
h_w^w
ρ_w
h_w^e
ρ_w
Water
h_c
ρ_c^w
h_c
ρ_c^e
Crust
h_l^w
h_m^w
ρ_m^w
h_l^e
h_m^e
ρ_m^e
Mantle
Lithosphere
h_a
ρ_a
Compensation Depth
Asthenosphere

A) Western Basin

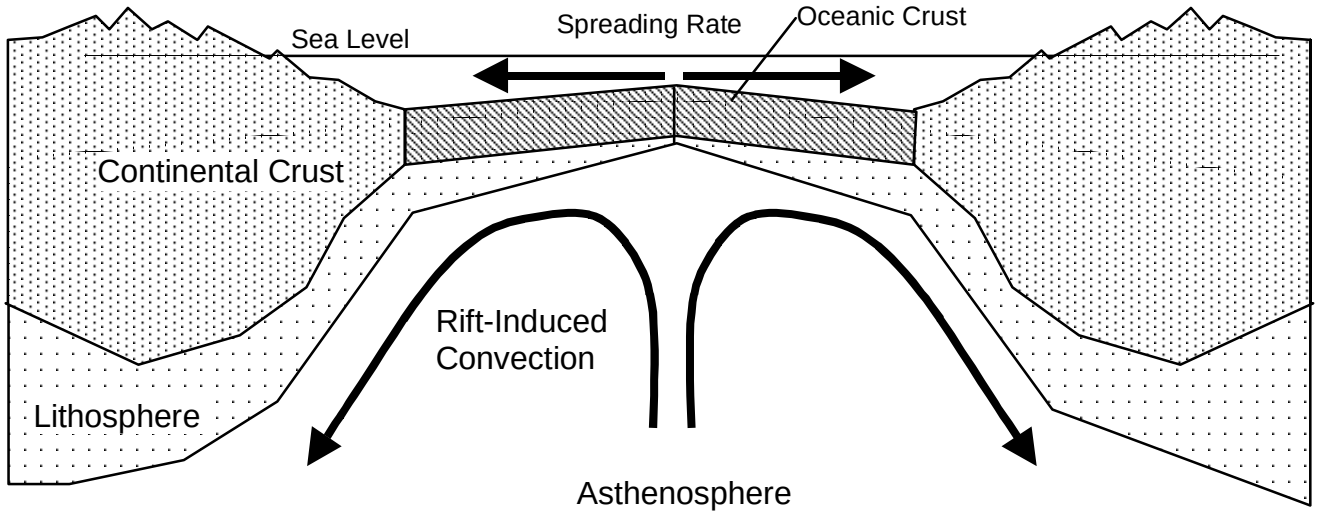

B) Eastern Basin